

1992

A Study of a Reimaging System for Correcting Large-Scale Phase Errors in Reflector Antennas

Eugene F. Lauria

University of Massachusetts Amherst

Follow this and additional works at: <https://scholarworks.umass.edu/theses>



Part of the [Electromagnetics and Photonics Commons](#), and the [Instrumentation Commons](#)

Lauria, Eugene F., "A Study of a Reimaging System for Correcting Large-Scale Phase Errors in Reflector Antennas" (1992). *Masters Theses 1911 - February 2014*. 1210.

Retrieved from <https://scholarworks.umass.edu/theses/1210>

This thesis is brought to you for free and open access by ScholarWorks@UMass Amherst. It has been accepted for inclusion in Masters Theses 1911 - February 2014 by an authorized administrator of ScholarWorks@UMass Amherst. For more information, please contact scholarworks@library.umass.edu.

1992

A Study of a Reimaging System for Correcting Large-Scale Phase Errors in Reflector Antennas

Eugene F. Lauria

Follow this and additional works at: http://scholarworks.umass.edu/masters_theses_2

This Open Access Thesis is brought to you for free and open access by the Dissertations and Theses at ScholarWorks@UMass Amherst. It has been accepted for inclusion in Masters Theses May 2014-current by an authorized administrator of ScholarWorks@UMass Amherst. For more information, please contact scholarworks@library.umass.edu.

**A STUDY OF A REIMAGING SYSTEM FOR CORRECTING
LARGE-SCALE PHASE ERRORS IN REFLECTOR ANTENNAS**

A Thesis Presented

by

EUGENE F. LAURIA

Submitted to the Graduate School of the
University of Massachusetts in partial fulfillment
of the requirements for the degree of

**MASTER OF SCIENCE
IN ELECTRICAL AND COMPUTER ENGINEERING**

September 1992

Department of Electrical and Computer Engineering

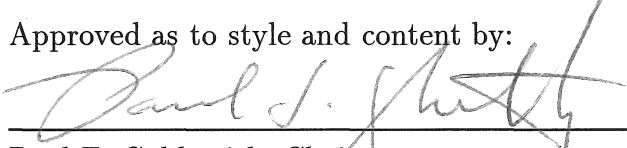
**A STUDY OF A REIMAGING SYSTEM FOR CORRECTING
LARGE-SCALE PHASE ERRORS IN RADIO ANTENNAS**

A Thesis Presented

by

EUGENE F. LAURIA

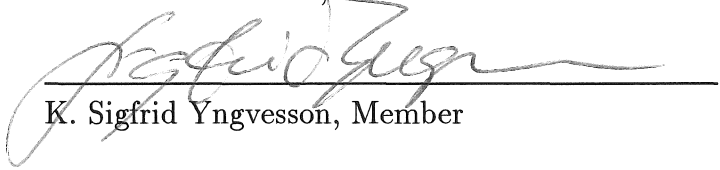
Approved as to style and content by:



Paul F. Goldsmith, Chair



Robert E. McIntosh, Member



K. Sigfrid Yngvesson, Member

Lewis E. Franks, Acting Department Head
Department of Electrical and Computer Engineering

ACKNOWLEDGMENTS

I would like to thank everyone who helped me with this thesis in any way. It would have been virtually impossible to complete this work without the help of others, and I have learned many valuable skills from all those who have worked with me during this project.

First of all, I would like to thank my advising committee for their instruction, help, and guidance. I have had the privilege of taking classes under each of my committee members, and I have found their classes to be extremely beneficial in my later studies and research. Specifically, I would like to thank my advisor Professor Paul F. Goldsmith. I consider myself extremely privileged to have worked with such a knowledgeable, patient, and helpful professor. His guidance has inspired me, and has given me the opportunity to find the work that I am truly devoted to. This has been a childhood goal, and Paul has helped me attain it. Also, I would like to thank Professor Robert E. McIntosh for his support in recommending me into the graduate program here at the University of Massachusetts. I have considered myself very fortunate in studying here as undergraduate and graduate student, and I would like to thank him for giving me the opportunity to continue my education as a graduate student. I hope that he feels that this work was worthy of his recommendation. I would also like to thank Professor K. Sigfrid Yngvesson. His suggestions in helping me with my research were extremely beneficial, and his guidance as an academic advisor was greatly appreciated. The entire staff at the Five College Radio Astronomy Observatory has been essential in helping me with my research. Specifically, I would like to extend my gratitude to Neal and

Ronna Erickson, and Ronald Grosslein for their technical support. They have shown me many useful technical skills and techniques. Also, thanks goes out to Thomas Scott, Todd Sunderland, and Kelly Smith for their help in manufacturing the components used in the experiment, John Krakala for helping me acquire the electronic components for the experiment, and special thanks goes to Maryanne Laukaitis for her help with the drafting and organization of the figures in the thesis. I would also like to thank LAMMDA lab for the use of their printed circuit board facility. I am greatly indebted to German Cortes and Jussi Tuovinen for their collaboration with the theoretical and mathematical aspects of this thesis. Their correspondence has helped me out of the many snags encountered during this project. Thanks goes out to Michael Rudenko for helping me with the many problems encountered in using LaTeX. Lastly, I would like to thank my parents. For without their love, support, and encouragement, none of this would have been possible.

ABSTRACT

A STUDY OF A REIMAGING SYSTEM FOR CORRECTING LARGE-SCALE PHASE ERRORS IN REFLECTOR ANTENNAS

SEPTEMBER 1992

EUGENE F. LAURIA,

B.S., UNIVERSITY OF MASSACHUSETTS

M.S., UNIVERSITY OF MASSACHUSETTS

Directed by: Professor Paul F. Goldsmith

This thesis investigates a new approach for dealing with the adverse effects of large scale deformations in the main reflector of a Cassegrainian antenna. In this method, the incident aperture distribution is imaged onto a tertiary focal plane. This is accomplished by using an optical imaging system consisting of a lens mounted behind the Cassegrain focus of the antenna. The lens forms a real image of the product of the incident aperture distribution and the pupil function of the antenna. The pupil function describes the profile of the main reflector of the antenna. If the incident aperture distribution is a plane wave, a real image of the pupil function of the main reflector will be produced at the focal plane of the image lens which would be the tertiary focus of the Cassegrainian system. Any imperfections in the main reflector of the antenna will be imaged onto the tertiary focal plane but over a smaller area as determined by the magnification of the system. In principle, if these errors are observable at the tertiary focal plane, an active correcting element placed in the tertiary focal plane may be installed to compensate for these errors, thus restoring the efficiency of the antenna. The

amplitude and phase of the electric field was measured at the image plane for a dielectric lens 152.4mm in diameter. Phase perturbations were simulated by using dielectric shims placed in the incident aperture plane. The phase of these shims in most cases, was measured to within 10° in the image plane. This degree of accuracy is quite adequate for correcting large-scale errors in the main reflector of the antenna.

TABLE OF CONTENTS

	Page
ACKNOWLEDGMENTS	iii
ABSTRACT	v
LIST OF FIGURES	ix
CHAPTER	
1. INTRODUCTION	1
2. RESEARCH PROGRAM	5
2.1 Description	5
2.2 Experimental layout	8
3. THEORY	16
3.1 Fourier Optical Theory of Lens Systems	16
4. RESULTS	25
5. DISCUSSION	37
6. CONCLUSION	44
APPENDIX: FOURIER OPTICS	46
A.1 Scalar Diffraction Theory	46
A.2 The Rayleigh–Sommerfeld diffraction theorem	52
A.2.1 The Sommerfeld Radiation Condition	55
A.3 The Fresnel and Fraunhofer approximations	57
A.4 Derivation of the Fourier transforming property of lenses	62
A.4.1 The lens thickness function	63
A.4.2 Fourier transforming properties of lenses	68
BIBLIOGRAPHY	73

LIST OF FIGURES

Figure	Page
1.1 Illustration of how a real image of the incident aperture distribution is obtained at the tertiary focus of a Cassegrainian antenna system.	3
1.2 Principle of imaging the incident aperture distribution of a Cassegrainian antenna onto a tertiary focal plane in order to correct for large-scale deformations on the main reflector.	4
2.1 Schematic of a Cassegrainian radio telescope optical system.	7
2.2 Illustration of the optical properties of the quasi-optical imaging system.	7
2.3 Schematic diagram of the apparatus used in the experiment.	10
2.4 Amplitude (a) and phase (b) of the aperture distribution incident on the objective lens.	11
2.5 Dielectric probe dimensions in inches (a), and E and H-plane power pattern (b) for the frequency used in this experiment.	14
3.1 Illustration of how a real image of the incident aperture distribution is formed.	18
4.1 Amplitude (a) and phase (b) of the Airy pattern produced by an aperture 150mm (6in) in diameter.	26
4.2 Phase of the electric field inside the main lobe of the objective lens inside, outside and in focus. Inside focus, the phase curves down, and outside focus, the electric field curves up. These measurements were taken in the focal plane of the objective lens.	27
4.3 Comparison between measured and theoretical values of the electric field in the focal plane of the objective lens.	29

4.4	Amplitude (a) and phase (b) of the real image of the incident aperture distribution measured at the focal plane of the image lens.	31
4.5	Amplitude (a) and phase (b) of the real image of a dielectric shim 76.2mm in diameter placed in the aperture plane of the objective lens. This shim is used to simulate a phase deviation of 50°.	33
4.6	Amplitude (a) and phase (b) of the real image of a dielectric shim 76.2mm in diameter with a tapered edge. The thickness of the shim produces a phase deviation of 78°.	34
4.7	Amplitude (a) and phase (b) of the real image of a dielectric square 76.2mm in length. The thickness of the square should produce a phase perturbation of 50°.	36
5.1	Calculated amplitude of the electric field incident on the lens for an aperture stop 76mm in diameter at a distance of 304.8mm behind the lens.	41
5.2	Comparison of the calculated electric field distribution incident on the objective lens between λ and $\lambda/10$	42
A.1	Surface used to describe the development of a diffraction theorem by using Green's theorem.	48
A.2	Surface used to account for the point discontinuity from the observation point in observing the electric field.	49
A.3	Screen and point sources used to derive the Rayleigh–Sommerfeld diffraction theorem.	53
A.4	Surface used in describing the Sommerfeld radiation condition.	56
A.5	Diffraction geometry for deriving the Fresnel and Fraunhofer approximations.	58
A.6	Lens thickness cross-section.	64
A.7	Illustration of the thickness function of the lens in terms of the radius of curvature.	66
A.8	Geometry for illustrating how a lens takes the Fourier transform of the incident aperture distribution.	69

CHAPTER 1

INTRODUCTION

In antenna systems employing reflecting surfaces, the adverse effects of errors in the figure of the main reflector are well known [1]. These effects introduce a variety of optical errors such as defocusing, coma, and astigmatism which reduce the efficiency of the antenna. Large antennas use panels which individually may be perfect, but may have setting errors and deformations. For reflector antennas that are fixed in position, this problem may be remedied by simply adjusting the panels of the main reflector in order to obtain the prescribed figure thus preserving the aperture efficiency of the antenna. For large steerable antennas, this problem is more complex since the structure of the antenna deforms under gravity. As the antenna is pointed to different elevations, the gravitational forces on the back structure change. As a result, the deformations of the main reflector are a function of elevation. Therefore, an active deformable surface is required to preserve the figure of the main reflector as the elevation of the antenna is changed.

A number of approaches have been employed to address this problem. For instance, a deformable secondary may be used as the correcting element [2], [3]. This approach is used in practice at the 140 ft. radio telescope at Green Bank, West Virginia. Another approach is adjustment of a segmented main reflector by computer

controlled actuators [4]. This approach has the virtue that an absolute measurement of the main reflector figure may be attained. If the panels are equipped with sensors on the edge of each segment, the relative position of each adjacent panel may be monitored and adjusted to attain the ideal figure that will maximize the aperture efficiency of the antenna. As the panels shift when the antenna is moved in elevation, their displacements may be measured and zeroed out by a control computer thus preserving the optimal figure of the antenna as it is pointed to different elevations. This technique is proving to be successful even at optical wavelengths as demonstrated by the system used on the 10-meter Keck telescope [5].

Implementation of a deformable primary or secondary reflector would be rather simple in the original design of an antenna. However, this approach may not be practical for an existing antenna, since it would require a complete redesign of the main reflector or subreflector and its back structure. This would be a very costly solution, and therefore, it would be extremely beneficial if there were another approach that would allow for the installation of an active surface without requiring the mechanical redesign of the antenna itself.

One approach that may prove to be useful would be to image the aperture onto a tertiary focal plane of the Cassegrain antenna. This may be achieved by placing a simple lens behind the Cassegrain focus of the antenna. Using the principles of Fourier optics, if a lens is placed at a distance of its focal length behind the Cassegrain focus (Figure 1.1), the resulting aperture distribution at the tertiary focus of the antenna will be a real image of the product of the incident aperture distribution and the pupil function (i.e. the function which describes the profile of

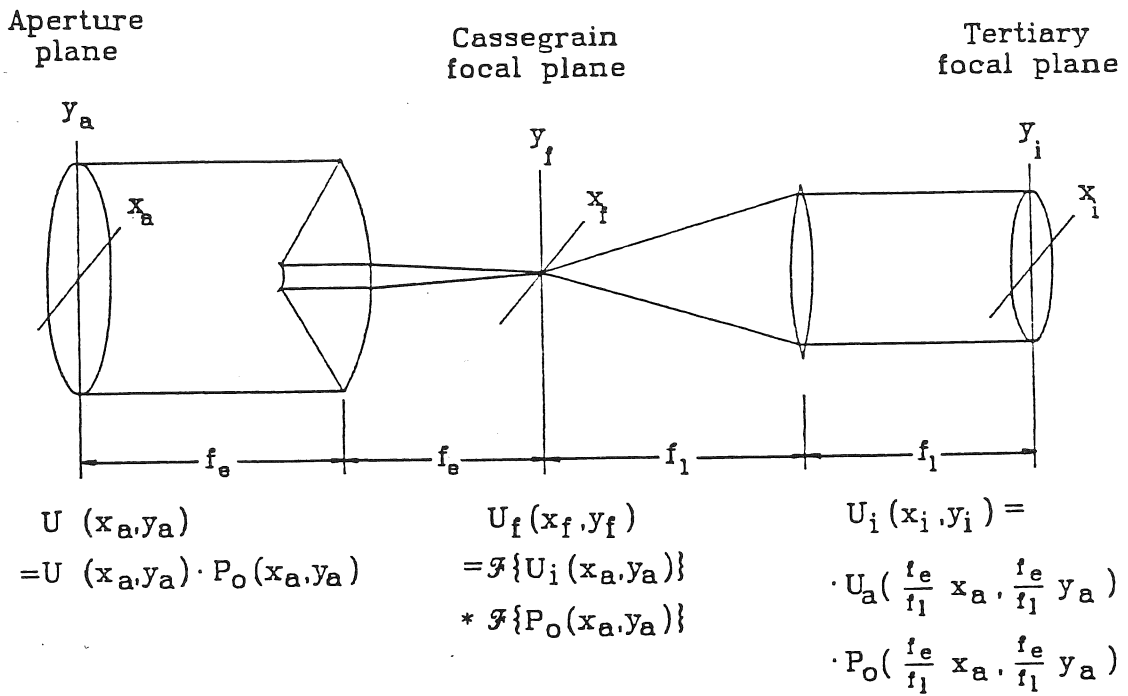


Figure 1.1 Illustration of how a real image of the incident aperture distribution is obtained at the tertiary focus of a Cassegrainian antenna system.

the main reflector), of the main reflector with both magnitude *and* phase preserved. If the antenna is illuminated by plane waves, a real image of the pupil function will exist at the tertiary focus. Any perturbations that may exist on the main reflector will be imaged onto a deformable quarternary mirror placed in the tertiary focus of the system as illustrated in Figure 1.2. The surface of the quarternary mirror could be deformed in such a manner as to form the conjugate surface of the main reflector, thus correcting for the phase perturbations in the main reflector. If the antenna is deformed by gravity, as it is changed in elevation, the quarternary reflector can then be adjusted to preserve the maximum efficiency of the antenna.

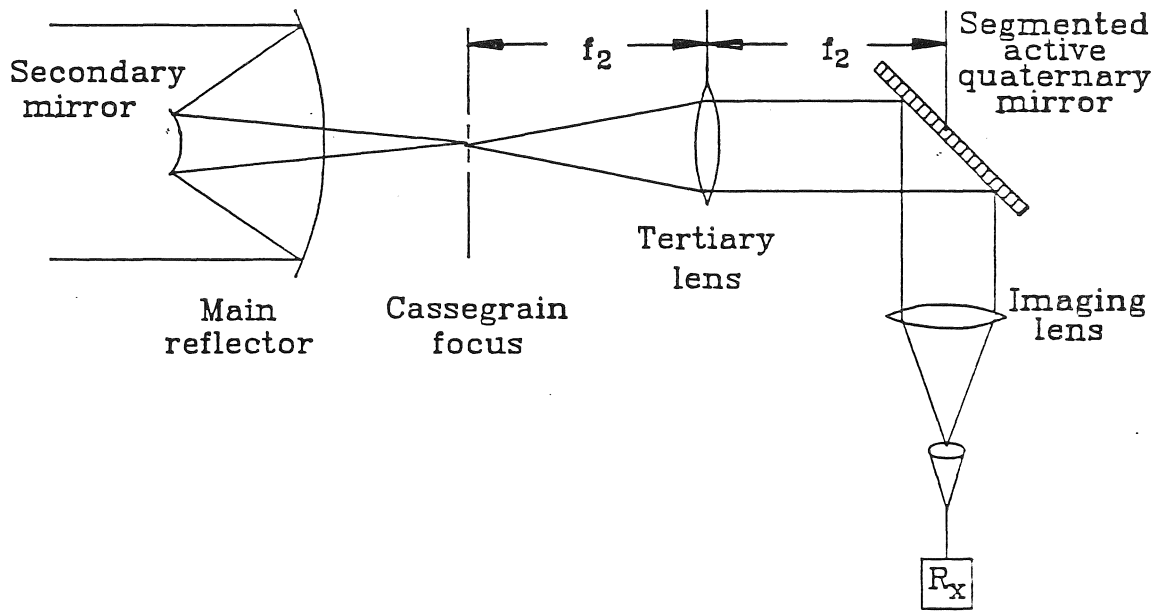


Figure 1.2 Principle of imaging the incident aperture distribution of a Cassegrainian antenna onto a tertiary focal plane in order to correct for large-scale deformations on the main reflector.

CHAPTER 2

RESEARCH PROGRAM

2.1 Description

The principal objective of this research program is to construct a real image of the incident aperture distribution of a lens, and to measure phase perturbations in the image plane which are placed in the aperture plane of the lens. The experiment will test the basic principles of Fourier optics to determine whether the incident aperture distribution can be successfully imaged onto a secondary focal plane. The intent of this experiment is to determine whether or not this scheme may be used in a system to correct large-scale deformations of the main reflector of a large radio antenna. The apparatus used in this experiment measures both magnitude and phase of the aperture distribution of the electric field at a frequency of 90.18 GHz or at a wavelength of 3.327mm.

The basic principle of the experiment may be described as follows: Through the principles of Fourier optics, the electric field distribution at the focal plane of a lens (or antenna), is found to be the convolution of the Fourier transforms of the incident aperture distribution and the pupil function of the lens [6]. The pupil function is a mathematical function that describes the aperture or profile of the

lens (see Figure 2.1). The convolution operation is denoted by $*$, and the Fourier transformation by \mathcal{F} , giving us

$$U_f(x_f, y_f) = \mathcal{F}\{U_a(x_a, y_a)\} * \mathcal{F}\{P(x_a, y_a)\}. \quad (2.1)$$

If the incident aperture distribution is a plane wave, its Fourier transform is a delta function. Therefore, at the focal plane of the lens, one would simply obtain the Fourier transform of the pupil function of the lens which is the classical Airy pattern for an unblocked circular aperture.

The imaging system consists of a single focusing element¹ located at a distance of its focal length behind the Cassegrain focus of the antenna. At the back focal plane of the lens (the tertiary focus), the incident aperture distribution and the pupil function of the antenna will be imaged over an area dictated by the magnification of the system. The magnification of the system is determined by taking the ratio of the focal lengths of the objective lens and the image lens, respectively. Referring to Figure 2.2,

$$U_i(x_i, y_i) = U_a\left(\frac{f_1}{f_2}x_a, \frac{f_1}{f_2}y_a\right) \cdot P\left(\frac{f_1}{f_2}x_a, \frac{f_1}{f_2}y_a\right), \quad (2.2)$$

where U_i is the aperture distribution of the electric field at the tertiary focal plane. Once the distribution of the electric field over the image plane is discerned, judgements about the design criteria may be made; such as which magnification will yield the smallest size correcting mirror and yet allow for enough resolution to

¹We can consider the focusing element as either a refractive or reflective element which is defined by a focal length f . For convenience, we will in general, refer to the imaging element as a lens.

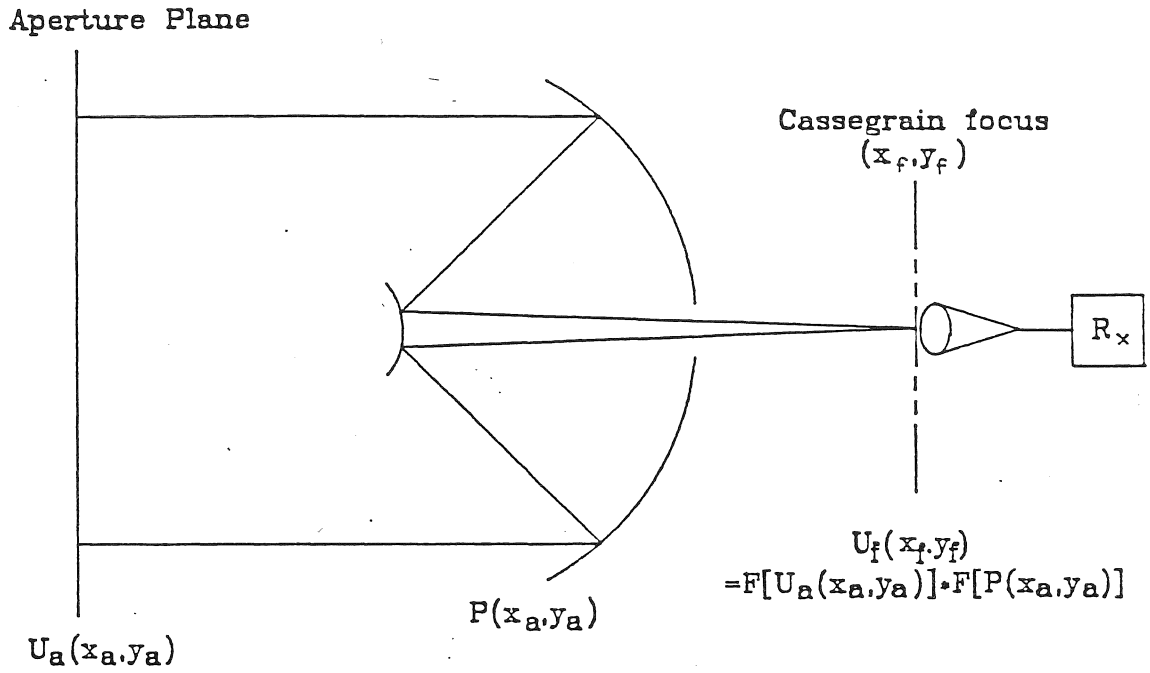


Figure 2.1 Schematic of a Cassegrainian radio telescope optical system.

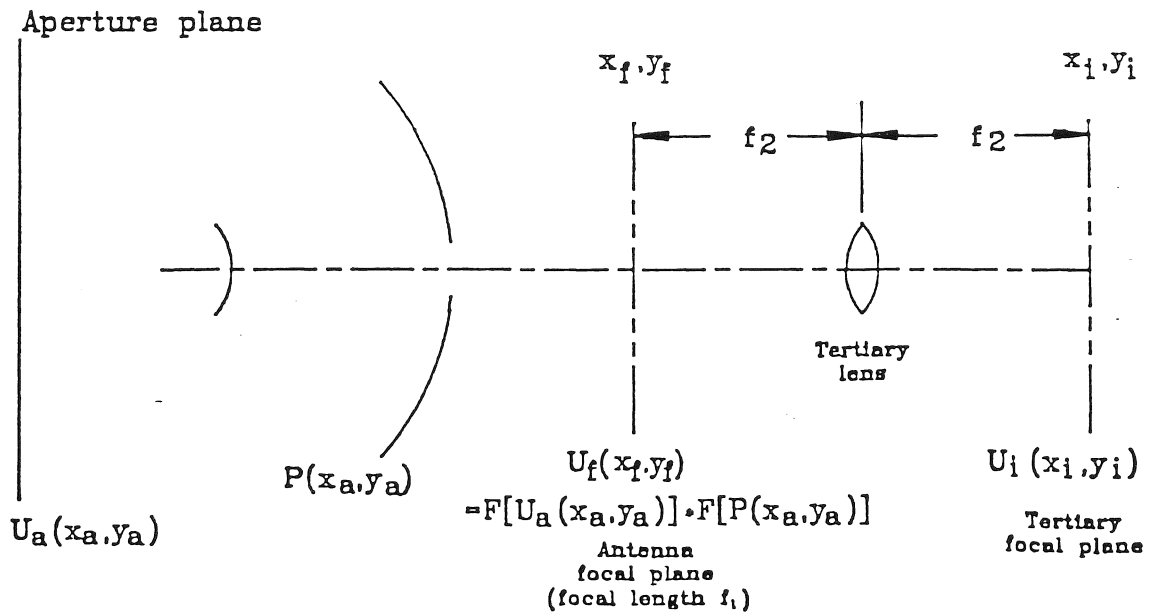


Figure 2.2 Illustration of the optical properties of the quasi-optical imaging system.

accurately reimage any phase perturbations over the incident aperture plane of the mirror.

An important factor in this approach is the magnification of the imaging system. The magnification dictates the size of the image of the antenna's aperture distribution. Because of diffraction, the errors cannot be scaled to any arbitrary size in the image plane. If the magnification is too high, the image will be projected onto a very small area, and the errors will not be able to be measured due to effects from diffraction. Conversely, if the magnification is too low, the image will be projected onto a very large area thus requiring an excessively large tertiary mirror. Another issue that will be addressed is the truncation effects of the imaging optics on the electric field distribution at the image plane. It has been found that the imaging lens' f-ratio should be at least equal to or less than that of the objective lens in order to avoid any vignetting effects of the aperture distribution in the focal plane.

2.2 Experimental layout

The apparatus used in this experiment is illustrated in Figure 2.3. Its operation may be described as follows: The measurements are performed at a frequency of 90.18 GHz ($\lambda = 3.327\text{mm}$). This signal is derived from a 10.12 GHz phase locked cavity tuned oscillator. The signal is sent through a mixer which produces upper and lower sidebands at 10.22 GHz and 10.02 GHz from the 100 MHz reference oscillator. The lower sideband is selected by a waveguide bandpass filter and then amplified by an X-band amplifier. The amplified signal is then sent through the

first stage tripler. The 30.06 GHz signal is sent through a Ka-band power amplifier which generated enough power to drive a second stage tripler so that 1 mW is obtained at the output of the tripler at 90.18 GHz. This signal is then transmitted by a scalar feedhorn.

To synthesize a collimated beam, the signal from the feedhorn passes through a 609.6mm diameter plano-convex lens which is made out of Rexolite. The lens was designed by a computer algorithm. In order to manufacture the lens, the depth of the curve was approximated in 0.381mm (0.015in) steps and the curved surface was milled on a rotary table whose radius for each step was dictated by the curve. The lens is illuminated with an 18 dB edge-taper. This distribution lowers diffraction effects at the edge of the lens and yet provides a 3 dB edge taper across the aperture of the objective lens. Measurements have shown (see Figure 2.4), phase variations of approximately $\pm 6^\circ$ and a 3 dB taper over the diameter of the objective lens with an amplitude ripple of the electric field of approximately 1.5 dB.

Although mismatch exists between the dielectric and air, it is found to be extremely difficult to match the collimating lens to free space. This is mainly because of the dielectric constant of the Rexolite and geometry of the lens. One attempt to improve the match of the lens is to mill circular grooves in the lens. This technique is found to be unsuccessful, due to excessive polarization effects in any plane other than the horizontal plane orthogonal to the optical axis of the lens.

After passing through the collimating lens, the beam approaches the objective lens. However, before reaching the objective lens, the beam passes through an aperture stop 152.4mm in diameter placed at a distance of the focal length in

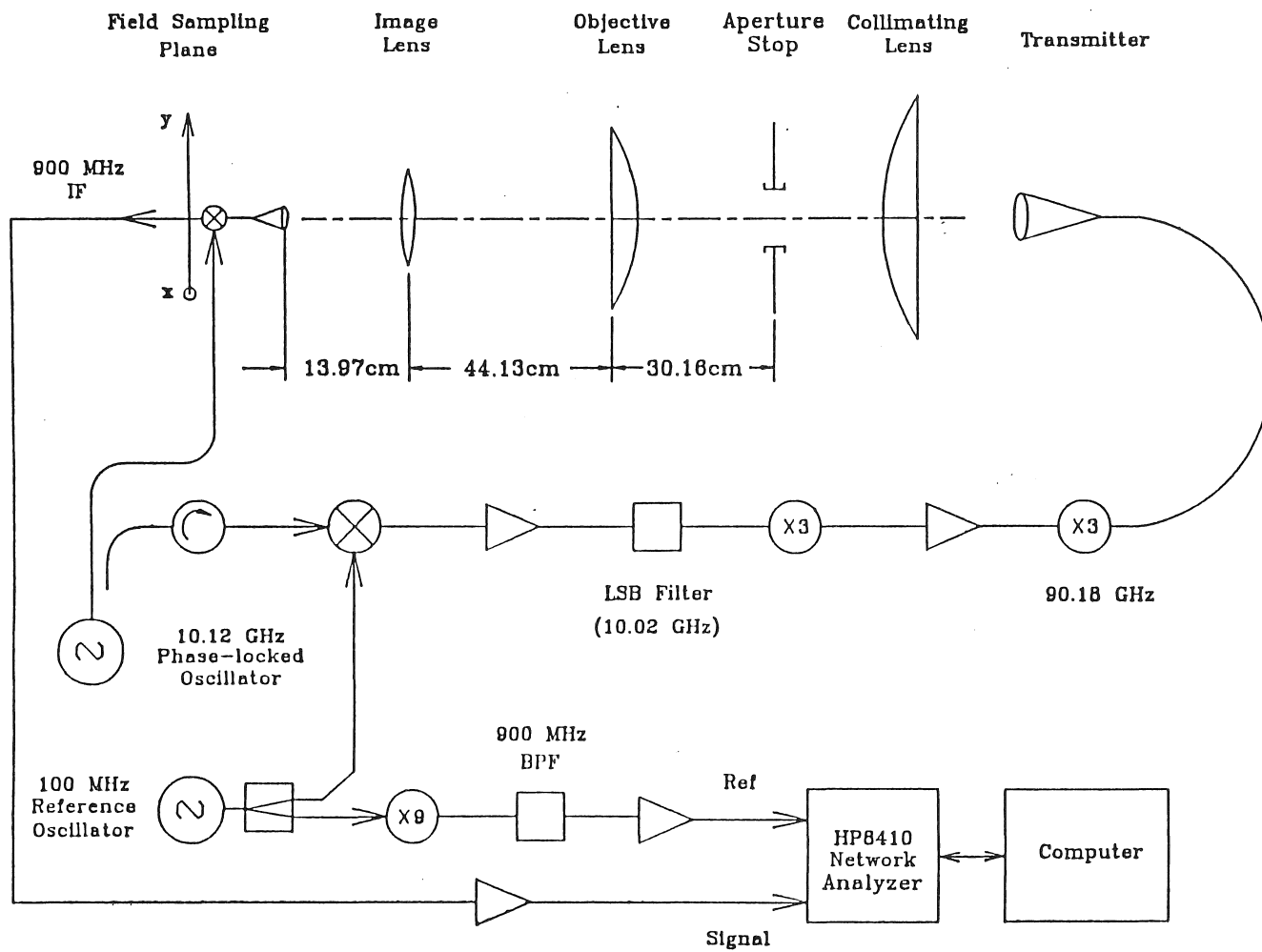
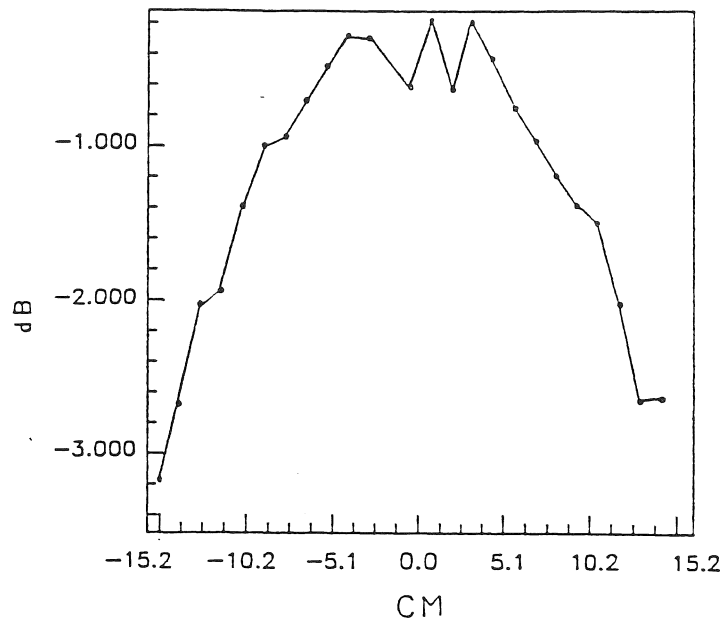
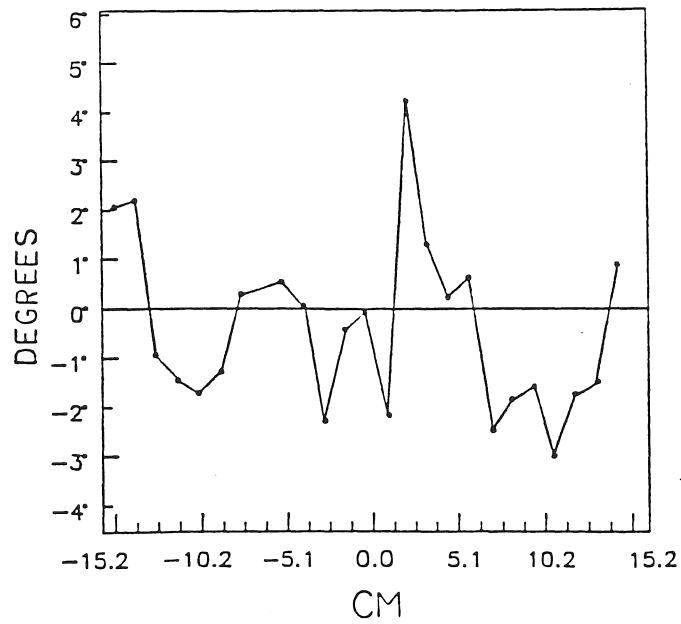


Figure 2.3 Schematic diagram of the apparatus used in the experiment.



(a)



(b)

Figure 2.4 Amplitude (a) and phase (b) of the aperture distribution incident on the objective lens.

front of the objective lens. As will be described in the chapter on the theory of the experiment, an aperture stop is necessary in order to take into account the finite size of the objective lens. Also, placing an aperture stop in the incident aperture plane puts the objective lens within the Fresnel region of the aperture. The objective lens is used to simulate the actual antenna under test.² The objective lens was made of the same material, and was manufactured in the same manner as the collimating lens. The specifications of the lens are a diameter of 304.8mm, with an f/D ratio equal to 1. In order to simulate phase perturbations on the surface of the objective lens, small shims of Rexolite were made with different thicknesses. The amount of phase in degrees these shims would introduce for a given thickness t and relative dielectric constant ϵ_r is given by the formula $\Delta\phi = \frac{360}{\pi}t(\sqrt{\epsilon_r} - 1)$. To measure the amplitude and phase of the shim in the image plane, the shim is adhered to a piece of Mylar in the aperture plane where the aperture stop is located. The image lens, which is a biconvex lens made of fused silica, has a diameter of 101.6mm with an f/D ratio of 1.375. This lens was located at a distance equal to the sum of the focal lengths of the objective lens and the image lens. The fused silica lens is matched to free-space with a quarter-wave polyethylene coating.

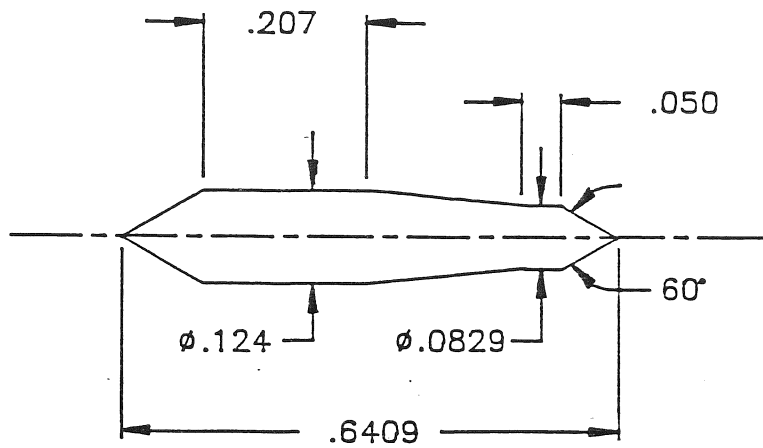
The electric field is measured in the image plane by the means of a dielectric probe made of teflon which feeds into a circular WR-10 waveguide. The design of the probe is based on a design described in [7], and was used to give a more isotropic power pattern than that of an open-ended waveguide. Its dimensions and E and H-plane power pattern is illustrated in Figure 2.5. Also, because of its

²Actually, a 12-inch Cassegrainian antenna was originally used, but this antenna was found to be defective and was not able to be used in the experiment.

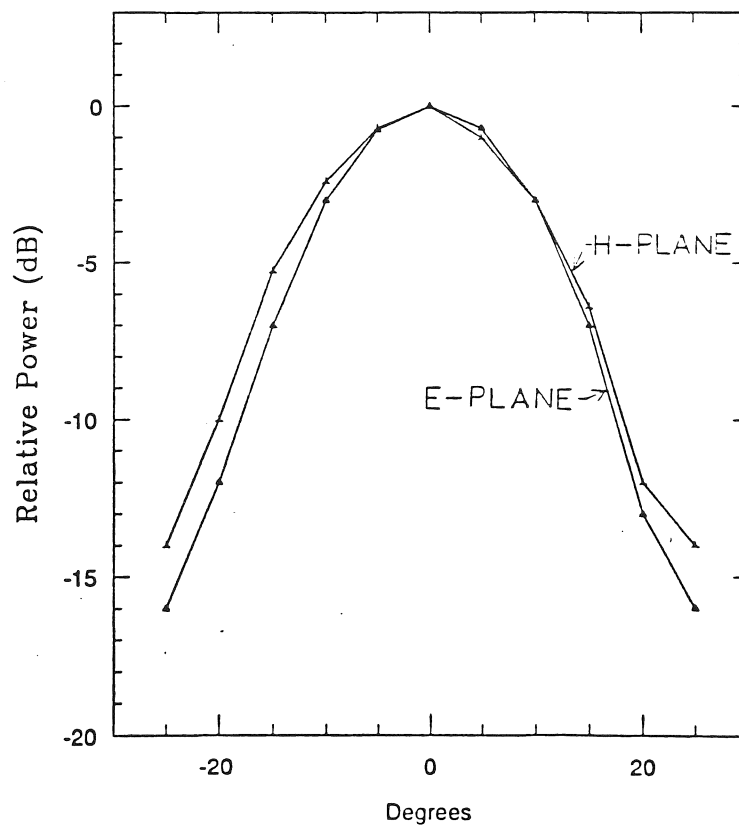
geometry and small size, the probe should not perturb the field it samples in any significant manner. Smoothing effects which would occur from a feed-horn of a larger aperture ought to be negligible. The probe is positioned in the focal plane of the image lens (139.7mm behind the center of the image lens). The probe is displaced by means of a computer-controlled stage which moves the probe in the image plane orthogonal to the propagation of the beam.

To measure the electric field distribution, the received 90.18 GHz signal is down-converted by a harmonic mixer whose 9th harmonic is used to mix to an intermediate frequency of 900 MHz. The pump oscillator whose 9th harmonic is used to down-convert the RF signal derived from the 10.12 GHz reference oscillator. To reduce loss and ensure phase stability, the pump to the harmonic mixer is sent through an X-band waveguide and then through a Gore-tex cable in order to allow flexibility between the stage and the waveguide but preserve phase stability. Calculations have shown that phase stability is 3° per degree Fahrenheit for the copper waveguide, and W.L. Gore specifies their cable to have no greater than 1° phase shift at 10 GHz when their cable is wrapped around a 50.8mm diameter mandrel.

The apparatus used to detect and display the electric field, is an HP8410B network analyzer which requires a reference signal in order to perform vectorial measurements. The IF going into the network analyzer 900 MHz. The reference signal is derived from the 100 MHz reference oscillator used to up-convert the 10.12 GHz oscillator. The 100 MHz signal is amplified and sent through a comb multiplier, and the 9th harmonic is extracted by a 900 MHz bandpass filter. This signal is then sent into the reference port of the network analyzer. The output voltages



(a)



(b)

Figure 2.5 Dielectric probe dimensions in inches (a), and E and H-plane power pattern (b) for the frequency used in this experiment.

for both amplitude and phase of the electric field from the network analyzer are measured by a computer-controlled voltmeter and are finally fed to the computer which controls the positioning of the stage and thus the probe.

CHAPTER 3

THEORY

3.1 Fourier Optical Theory of Lens Systems

To illustrate the Fourier transforming property of a lens and how a real image of the incident aperture distribution is formed at the image plane, scalar diffraction theory is used to analyze the electric field distribution at the different focal planes of the system. Two particularly good references on the discussion of diffraction theory can be found in [6] and [8], and the derivation of the Fourier transforming properties of lenses through scalar diffraction theory is shown in the appendix. The scheme used to illustrate how the incident aperture distribution is imaged onto the tertiary focal plane is illustrated in Figure 3.1. The imaging system is illuminated by plane waves characterized by $U_i(\vec{r}_a)$, which are incident towards the aperture plane of the objective lens. The aperture distribution in the aperture plane is represented by $U_a(\vec{r}_a)$ which is initially, an unbounded function. The profile of the objective lens is described by the pupil function $P_o(\vec{r}_l)$ and is a finite function. The finite size of the lens is taken into account by projecting the pupil function of the objective lens onto the aperture plane. This then defines the aperture distribution $U_a(\vec{r}_a)$, as the product of the incident electric field distribution $U_i(\vec{r}_a)$ and the pupil

function of the objective lens $P_o(\vec{r}_l)$. This relationship implies that the aperture distribution $U_a(\vec{r}_a)$ is now a finite function (because the pupil function is a finite function), and the lens is treated as though it is infinite in extent. However, this is an approximation, and the physical interpretation of this mathematical abstraction is subtle. This abstraction implies that an aperture stop has to be placed in the aperture plane. Also, the diameter of the lens has to be much larger than the aperture stop in order to take into account diffraction effects from the edge of the aperture stop.¹ The position vector \vec{r} is characterized as $\hat{x}x + \hat{y}y$. The focal plane of the lens, is denoted by the (x_f, y_f) plane, and the electric field distribution there is represented by the function $U_f(\vec{r}_f)$. The objective lens has a focal length f_1 . The imaging lens with focal length f_2 , is located at a distance equal to the sum of the focal lengths behind the objective lens. Both lenses are approximated as being thin lenses. Finally, the image plane is located in the focal plane of the imaging lens where the image aperture distribution is represented by the function $U_{im}(\vec{r}_i)$. It will be illustrated that a real image of the incident aperture distribution and the pupil function is formed at the image plane. A real image is defined as an image that preserves *both* amplitude and phase of the incident aperture distribution. Even though this derivation is being applied to a lens, the same relationship may be applied to aperture antennas without any loss of generality since aperture antennas perform the same function for radio waves as lenses traditionally do for shorter wavelength electromagnetic radiation.

¹It was found in this experiment that for an aperture stop 76.2mm in diameter, the edge-taper for a 304.8mm dia. f/1 lens was approximately 20dB at a distance of its focal length behind the aperture stop.

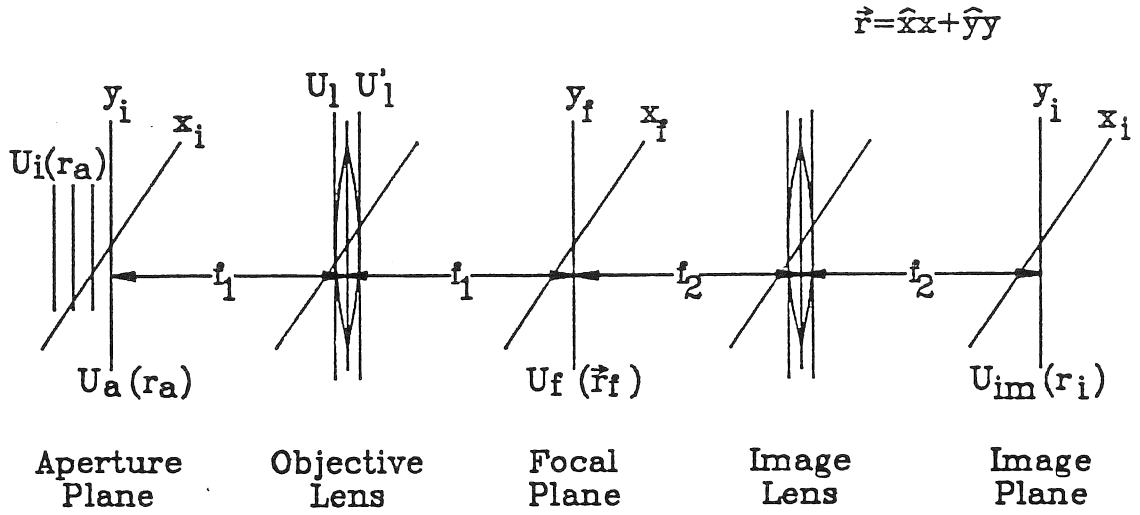


Figure 3.1 Illustration of how a real image of the incident aperture distribution is formed.

Using the Rayleigh–Sommerfeld diffraction formula and assuming that the objective lens is in the Fresnel region of the aperture plane for an aperture of the same diameter of the objective lens, the aperture distribution on the front surface of the lens may be expressed as

$$U_l(\vec{r}_l) = \frac{e^{jkf_1}}{j\lambda f_1} \int_{-\infty}^{\infty} U_a(\vec{r}_a) e^{j\frac{k}{2f_1}|\vec{r}_l - \vec{r}_a|^2} d\vec{r}_a. \quad (3.1)$$

In the appendix, a direct Fourier transform relationship was established between the aperture plane distribution $U_a(\vec{r}_a)$ and the aperture distribution at the focal plane of the objective lens $U_f(\vec{r}_f)$

$$U_f(\vec{r}_f) = \frac{e^{j2kf}}{j\lambda f} \mathcal{F}\{U_a(\vec{r}_a)\} \quad (3.2)$$

Recall that in order to take into account the finite diameter of a lens, the aperture distribution $U_a(\vec{r}_a)$ is characterized as the product of the incident aperture distribution $U_i(\vec{r}_a)$ and the pupil function of the objective lens $P_o(\vec{r}_a)$. This relationship implies that the aperture distribution $U_a(\vec{r}_a)$ is a bounded function and that the lens is now infinite in diameter. However, this is an approximation using geometrical optics which assumes that the electric field drops to zero at the edge of the aperture. The theory of Fourier optics is usually derived in the context of optical wavelengths [6], [8] where certain approximations in diffraction theory are assumed (i.e. geometrical optics). These approximations would imply that for a given aperture at optical wavelengths, the intensity at the edge of the aperture is assumed to drop to zero at the edge of the aperture. With this assumption, the lens' shadow is projected onto the incident aperture plane, and since the electric field drops to zero outside the edge of the lens, the lens only has to be the size of the aperture. This may be a valid approximation in the case of optical wavelengths where the wavelength of light is much smaller than that of the aperture, but for millimeter waves for the same given aperture, this assumption is no longer valid. Diffraction theory dictates that the electric field does not drop off to zero at the edge of the aperture stop, but has a gradual edge-taper. This implies that the diameter of the lens has to be larger than the diameter of the aperture stop in order for all the energy to pass through the lens and not introduce any edge effects. Equation (3.7), is derived for optical wavelengths and assumes that the effects of diffraction are not severe. Since this is not a valid approximation for millimeter wavelengths with smaller apertures, the theory of Fourier optics may have

some problems in describing some effects that will be observed in the image plane of the system. Namely, edge effects seen from the edge of the optics and phase shims. To more accurately describe these phenomena, more rigorous calculations are required where the diffraction integrals derived from the Rayleigh–Sommerfeld diffraction formula are solved numerically. However, for larger apertures at millimeter wavelengths, the effects from diffraction ought to become less bothersome, and the theory of Fourier optics should be a more accurate tool in describing the electric field distribution in the image plane of the system. But when applying the principles of Fourier optics towards larger apertures, one has to make sure that *the focal plane of the lens or antenna is still within the Fresnel region*. As the aperture increases, so does the distance to the Fresnel region. The distance to the Fresnel region where for an aperture of diameter D is $\sqrt[3]{\frac{\pi D^4}{64\lambda}}$. If the focal length of the lens or antenna is less than this quantity, the binomial approximation used in deriving the Fresnel approximation may no longer be valid. This approximation is the basis from which the principles of Fourier optics are derived. If the Fresnel approximation is not valid, the higher order terms in the binomial expansion of the phase term in the diffraction integral cannot be ignored. Therefore, the diffraction integral has to be solved numerically in order to achieve an accurate result.

In taking the finite diameter of the lens into account, the aperture distribution $U_a(\vec{r}_a)$ is expressed as the product of the incident aperture distribution $U_i(\vec{r}_a)$ with the pupil function of the objective lens $P_o(\vec{r}_a)$, the Fourier transform relationship at the focal plane of the lens is now found to be the *convolution of the Fourier*

transforms of the incident aperture distribution $U_i(\vec{r}_i)$ and the pupil function $P_o(\vec{r}_i)$ of the objective lens. This relationship is derived as follows:

$$\begin{aligned}
U_f(\vec{r}_f) &= \frac{e^{j2kf_1}}{j\lambda f_1} \mathcal{F} \{U_a(\vec{r}_a)\} \\
&= \frac{e^{j2kf_1}}{j\lambda f_1} \mathcal{F} \{U_i(\vec{r}_a) \cdot P_o(\vec{r}_a)\} \\
&= \frac{e^{j2kf_1}}{j\lambda f_1} \mathcal{F} \{U_i(\vec{r}_a)\} * \mathcal{F} \{P_o(\vec{r}_a)\} \tag{3.3}
\end{aligned}$$

If the incident aperture distribution $U_i(\vec{r}_a)$ is characterized by a plane wave, and the pupil function $P_o(\vec{r}_a)$ represents a circular aperture, one ends up with the classical Airy pattern at the focal plane of the imaging system. The convolution nature represented in eq. (3.4) implies a smoothing of the incident aperture distribution [6]. This in effect, lowers the resolution of the incident aperture distribution. By studying the characteristics of the Airy pattern, it is known that as the aperture of the objective lens increases, the size of the Airy disc decreases. Therefore, in order to obtain the highest resolution of the incident aperture distribution, the diameter of the objective lens should be as large as possible. Because of this relationship, large aperture telescopes are used extensively in the astronomical community in order to achieve high resolution of astronomical sources they observe.

The Fourier transform relationship derived between the aperture distribution $U_a(\vec{r}_a)$ and the aperture distribution in the focal plane of the objective lens $U_f(\vec{r}_f)$, exists between the image plane aperture distribution $U_{im}(\vec{r}_i)$ and the focal plane aperture distribution $U_f(\vec{r}_f)$. Analogously from eq. (3.7), the aperture distribution

at the image plane of the system, $U_{im}(\vec{r}_i)$ may be expressed as the Fourier transform of the focal plane aperture distribution $U_f(\vec{r}_f)$:

$$U_{im}(\vec{r}_i) = \frac{e^{j2kf_2}}{j\lambda f_2} \mathcal{F} \{U_f(\vec{r}_f)\}. \quad (3.4)$$

Substituting in the expression for focal plane aperture distribution $U_f(\vec{r}_f)$ from eq. (3.7), the resulting expression involves a nested group of Fourier transforms:

$$\begin{aligned} U_{im}(\vec{r}_i) &= -\frac{e^{j2k(f_1+f_2)}}{\lambda^2 f_1 f_2} \mathcal{F} \{ \mathcal{F} \{U_a(\vec{r}_a)\} \} \\ &= -\frac{e^{j2k(f_1+f_2)}}{\lambda^2 f_1 f_2} \int_{-\infty}^{\infty} \left\{ \int_{-\infty}^{\infty} U_a(\vec{r}_a) e^{-j\frac{k}{f_1}\vec{r}_a \cdot \vec{r}_f} d\vec{r}_a \right\} e^{-j\frac{k}{f_2}\vec{r}_f \cdot \vec{r}_i} d\vec{r}_f \end{aligned} \quad (3.5)$$

Breaking down the position vectors into their components and interchanging the order of integration, the aperture distribution at the image plane is expressed as

$$\begin{aligned} U_{im}(x_i, y_i) &= -\frac{e^{j2k(f_1+f_2)}}{\lambda^2 f_1 f_2} \iint_{-\infty}^{\infty} \left\{ \iint_{-\infty}^{\infty} U_a(x_a, y_a) dx_a dy_a \right\} \\ &\quad \cdot e^{-j\frac{k}{f_1}x_f(x_a + \frac{f_1}{f_2}x_i)} e^{-j\frac{k}{f_1}y_f(y_a + \frac{f_1}{f_2}y_i)} dx_f dy_f \end{aligned} \quad (3.6)$$

Letting,

$$\tilde{x}_f = \frac{x_f}{\lambda f_1}; \quad \tilde{y}_f = \frac{y_f}{\lambda f_1}$$

$$d\tilde{x}_f = \frac{dx_f}{\lambda f_1}; \quad d\tilde{y}_f = \frac{dy_f}{\lambda f_1} \quad (3.7)$$

$$U_{im}(x_i, y_i) = -\frac{f_1}{f_2} e^{j2k(f_1+f_2)} \iint_{-\infty}^{\infty} \left\{ \iint_{-\infty}^{\infty} U_a(x_a, y_a) dx_a dy_a \right\} \\ \cdot e^{-j2\pi\tilde{x}_f(x_i + \frac{f_1}{f_2}x_i)} e^{-j2\pi\tilde{y}_f(y_i + \frac{f_1}{f_2}y_i)} d\tilde{x}_f d\tilde{y}_f \quad (3.8)$$

Recognizing that the outer integral is a delta function, we get

$$U_{im}(x_i, y_i) = -\frac{f_1}{f_2} e^{j2k(f_1+f_2)} \iint_{-\infty}^{\infty} \{U_a(x_a, y_a)\} \\ \cdot \delta(x_a + \frac{f_1}{f_2}x_i) \delta(y_a + \frac{f_1}{f_2}y_i) dx_a dy_a \quad (3.9)$$

From this, we finally obtain

$$U_{im}(x_i, y_i) = -\frac{f_1}{f_2} e^{j2k(f_1+f_2)} [U_a(-\frac{f_1}{f_2}x_i, -\frac{f_1}{f_2}y_i)] \quad (3.10)$$

Recall that in order to take into account the finite size of the objective lens, the aperture distribution $U_a(\vec{r}_a)$ is expressed as the product of the incident aperture distribution $U_i(\vec{r}_a) \cdot P_o(\vec{r}_a)$. Therefore at the image plane the aperture distribution may now be expressed as

$$U_{im}(x_i, y_i) = -\frac{f_1}{f_2} e^{j2k(f_1+f_2)} [U_i(-\frac{f_1}{f_2}x_i, -\frac{f_1}{f_2}y_i) \cdot P_o(-\frac{f_1}{f_2}x_i, -\frac{f_1}{f_2}y_i)] \quad (3.11)$$

If the incident aperture distribution $U_i(\vec{r}_i)$ is a plane wave, one will obtain a magnified image of the pupil function of the objective lens in the image plane of the

system. Any errors that may exist on the surface of the objective lens (or the main reflector of the antenna), would be quantified by the pupil function $P_o(\vec{r}_a)$. Therefore, a real image of these errors will exist at the image plane of the system assuming that these errors are large enough so that diffraction effects are not significant.

Finally, the finite size of the image lens is taken into account by projecting its pupil function $P_i(\vec{r}_i)$ onto the image plane. Mathematically, this is represented by simply multiplying the pupil function of the image lens with equation (3.16).

$$U_{im}(x_i, y_i) = -\frac{f_1}{f_2} e^{j2k(f_1+f_2)} P_i(x_i, y_i) \times [U_i(-\frac{f_1}{f_2}x_i, -\frac{f_1}{f_2}y_i) \cdot P_o(-\frac{f_1}{f_2}x_i, -\frac{f_1}{f_2}y_i)] \quad (3.12)$$

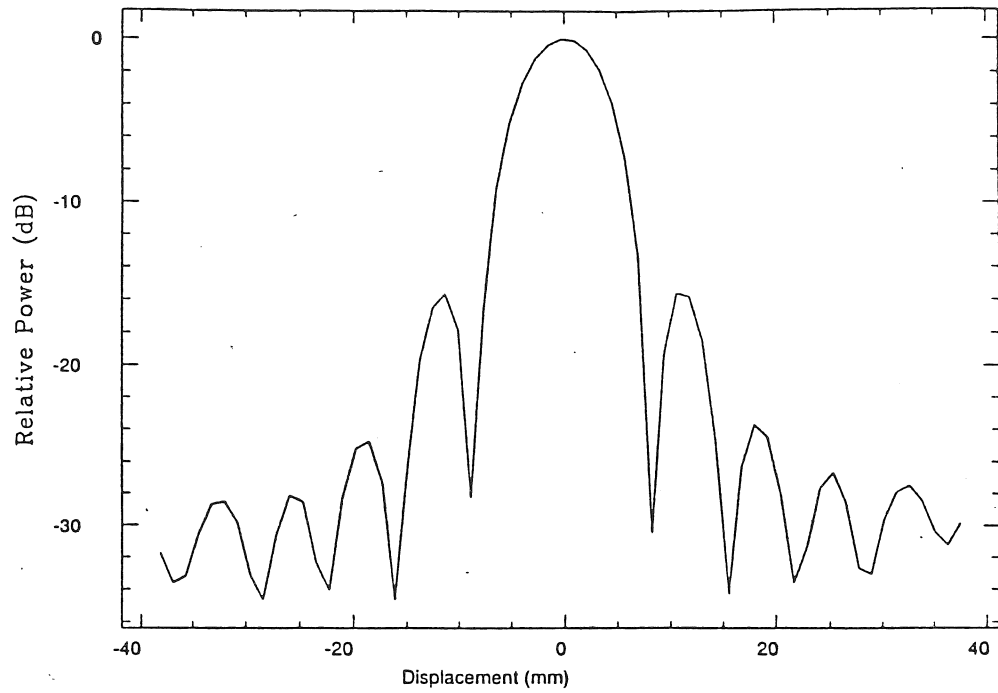
This result implies that a real image of the incident aperture distribution is formed in the image plane. This result is unique because it preserves both magnitude and phase of the incident aperture distribution and the pupil function of the objective lens. Therefore, any phase perturbations that may exist on the surface of the objective lens will be imaged in the image plane. Mathematically, these perturbations would be quantified by the pupil function of the image lens. As a result, a deformable correcting surface could be installed at the focal plane of the image lens whose surface could be adjusted to form the conjugate surface of the deformed main reflector of the antenna. This correction will preserve the ideal figure of the antenna, and preserve its maximum aperture efficiency as it is changed in elevation.

CHAPTER 4

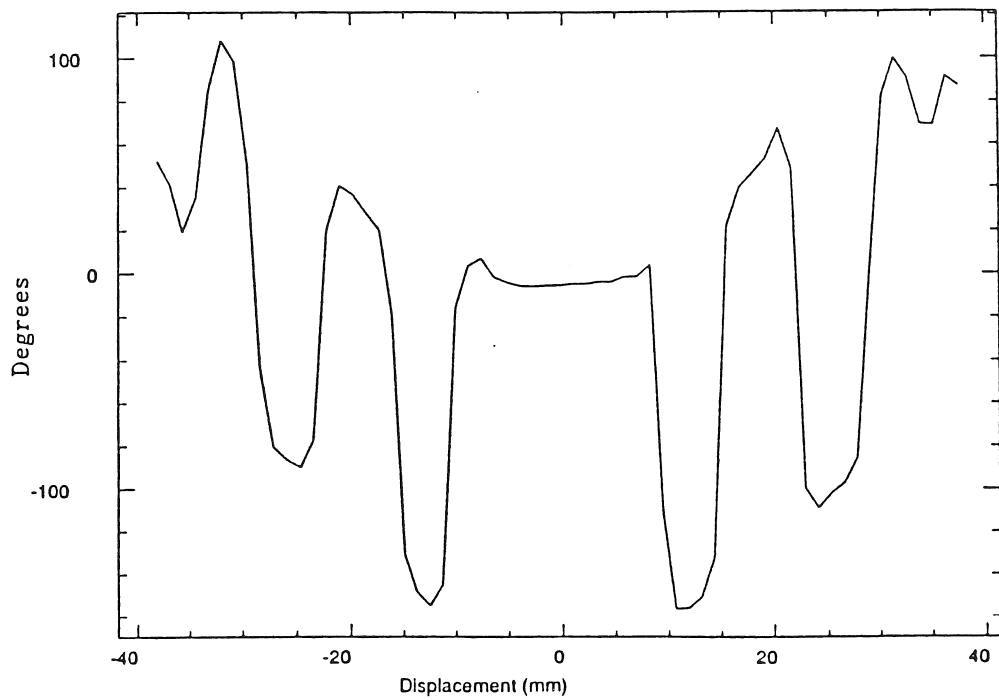
RESULTS

In trying to image the incident aperture distribution it was found that the alignment of the optics is critical. Precise positioning of the optics both laterally and axially is necessary in order to obtain any meaningful measurements. To determine the focal length of the objective and image lenses, the phase of the electric field was measured in the region of the main lobe of the Airy pattern for each lens with a plane wave illumination. As illustrated in Figure 4.1, when the lens is in focus, the phase of the electric field is flat, and the deepest nulls in amplitude occur across the main lobe of the airy pattern. If the lens is not in focus, the phase either curves up if the lens is inside of the focus, or curves down if the lens is outside of the focus. This effect is illustrated in figure 4.2. The curvature arises from the quadratic phase term in the diffraction integral describing the electric field in this region. From these measurements, the objective lens was found to have a focal length of 301.625mm as measured from the flat side of the lens. The image lens was found to have a focal length of 139.7mm as measured from its center.

In order to observe how well the apparatus performs in measuring the electric field, the aperture distribution of the electric field was measured at the focal plane of the objective lens. After measuring the electric field, the results were compared to



(a)



(b)

Figure 4.1 Amplitude (a) and phase (b) of the Airy pattern produced by an aperture 150mm (6in) in diameter.

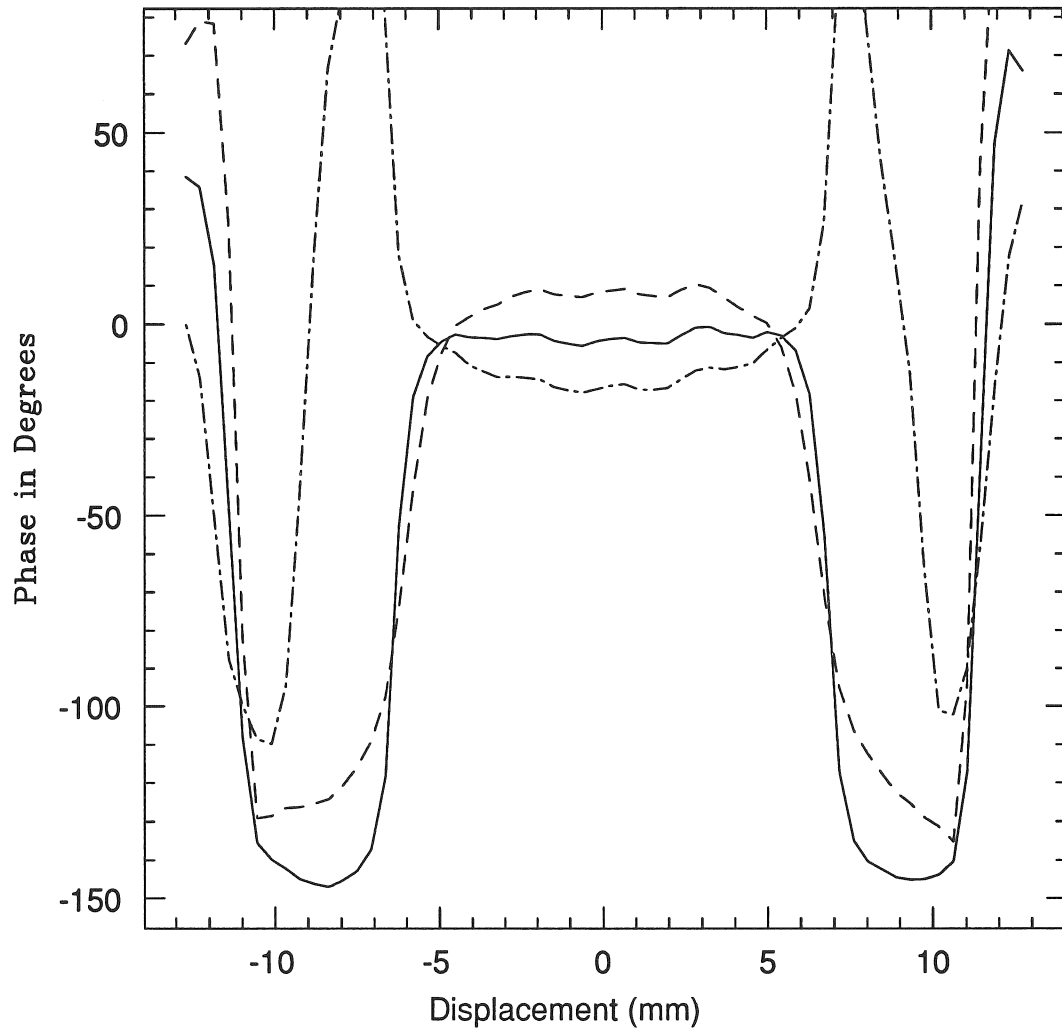


Figure 4.2 Phase of the electric field inside the main lobe of the objective lens inside, outside and in focus. Inside focus, the phase curves down, and outside focus, the electric field curves up. These measurements were taken in the focal plane of the objective lens.

those predicted from a computer model. The results are displayed in Figure 4.3 and show fairly good agreement between the measured electric field and the calculated results. The residual errors arise from errors in modelling the edge taper of the electric field illuminating the lens and effects from edge diffraction in the aperture which are not accounted for in the computer model. The model basically performs a Fourier transform of the incident aperture distribution which drops to zero at the edge of the aperture. This does not take into account the effects of edge diffraction because in the model it is assumed that the electric field drops to zero at the edge of the aperture.

Initially, the electric field was measured in the image plane without any obstructions. This measurement shows how the incident aperture distribution is imaged onto the image plane. If the apparatus works properly, the aperture distribution at the image plane should be a magnified image of the pupil function of the lens. For the configuration used in the experiment, the magnification of the system was 2.16. The magnification is determined by taking the ratio of the focal length of the objective lens and dividing it by the focal length of the image lens. The diameter of the image of the incident aperture distribution, known as the exit pupil, is determined by the diameter of the aperture divided by the magnification. As a result, the diameter of the image should be 2.16 times smaller than its original size in the aperture plane with very little phase variation across the image. The results of these measurements are shown in figure 4.4 which shows the image of the pupil function of the objective lens in terms of both magnitude and phase. The diameter of the image was found to be 67.1mm with a maximum phase deviation

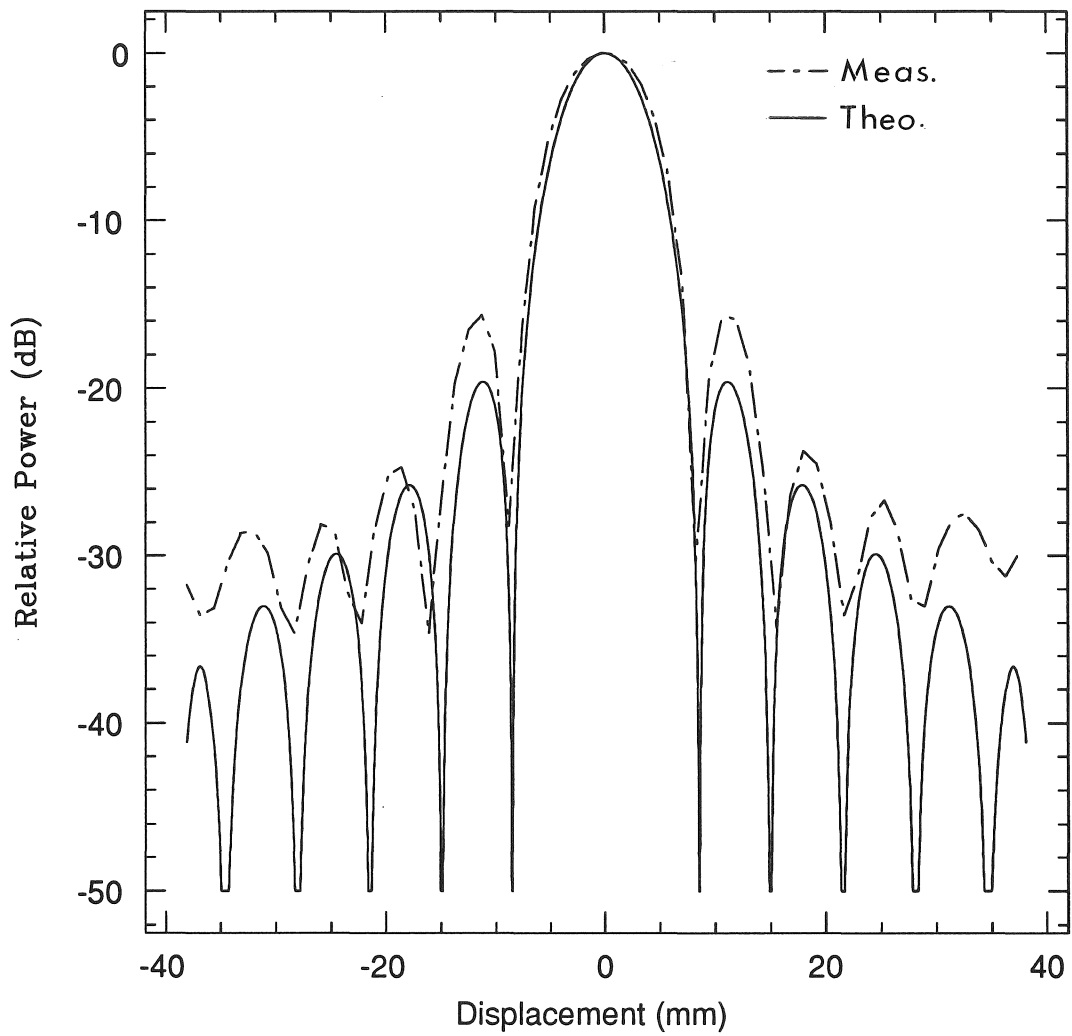


Figure 4.3 Comparison between measured and theoretical values of the electric field in the focal plane of the objective lens.

of about 11° near the center. The phase of this measurement was subtracted from the other phase measurements in the experiment in order to remove any residual errors in the system.

Several measurements were made with various dielectric shims placed in the aperture plane of the system. The shims were held in place by adhering them to a thin sheet of mylar by rubber cement in the aperture plane where the aperture stop is located. The shims were of different sizes and thicknesses in order to simulate various phase perturbations on the surface of the lens. The first shim measured was a disk made of Rexolite 76.2mm in diameter whose thickness produces a phase deviation of 50° . The results of this measurement in terms of both amplitude and phase are shown in Figure 4.5. Measurements show that the phase is measured to within 10° of accuracy. A discrepancy arises in the measurement of the amplitude of the shim. Upon examining the image of the amplitude distribution of the shim, one observes that the presence of the disk's edge is clearly seen. This result is inconsistent with the prediction of Fourier optical theory. Since the shim acts only as a phase perturbation, Fourier optical theory would predict that its image should show up only as a phase perturbation and not affect the amplitude in any way. Strictly speaking, the shim does cause some perturbation in amplitude because of the mismatch between the shim and free-space. However, the contribution from mismatch are far less than what is measured. It is believed that these ripples arise from edge diffraction caused by the sharp edges of the disk. The abrupt change from the edge of the disk diffracts the electric field, which initially propagates normal to the surface of the shim, into different angles of propagation. It is believed that

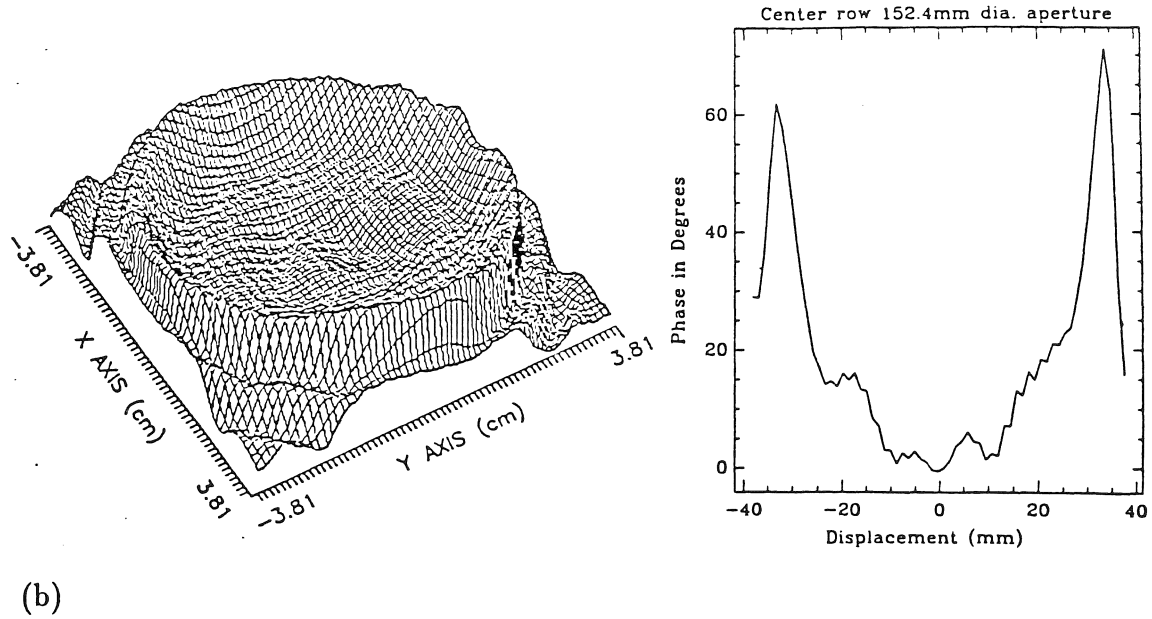
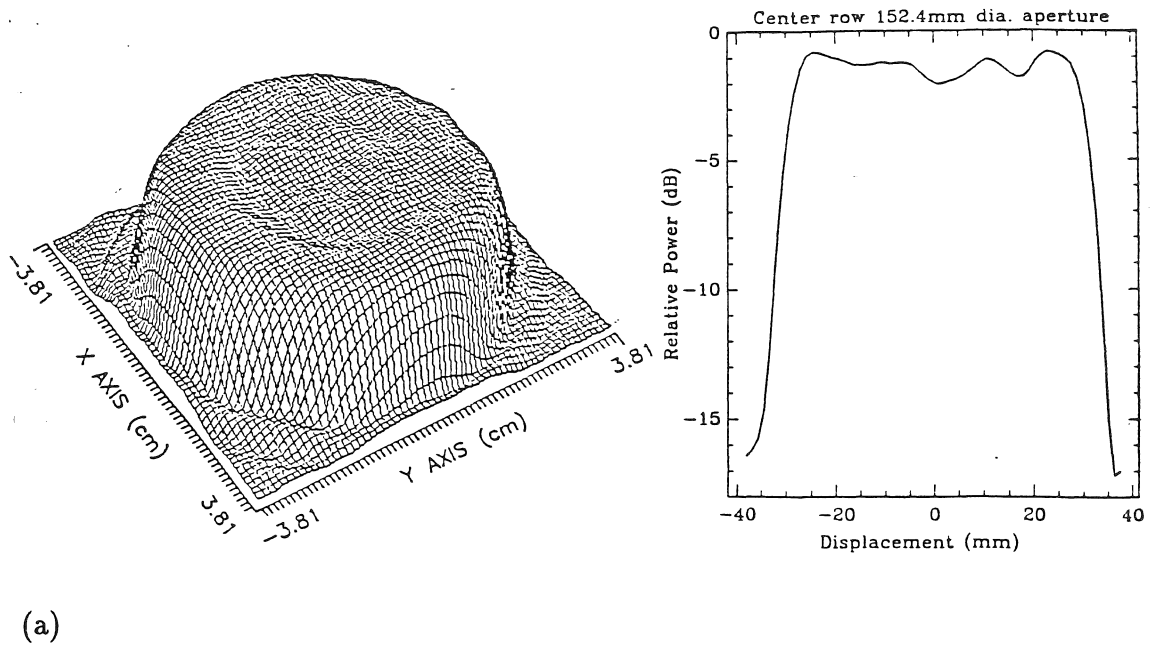


Figure 4.4 Amplitude (a) and phase (b) of the real image of the incident aperture distribution measured at the focal plane of the image lens.

these diffracted waves interfere with each other thus causing the ripples seen in the image plane, and thus, detected by the probe. In an attempt to reduce this effect, the edge of the disk was tapered so that the transition from the dielectric to air was less abrupt. This should lower the diffraction of the electric field at the edge and therefore, should produce fewer ripples in the measurements. The results of this modification are shown in Figure 4.6, which is for a disk 76.2mm in diameter and 1.22mm thick, which should yield a phase shift of 78° . Compared with the results of the disk with the abrupt edge (Figure 4.5), one observes that the edge effect is still present at the edge of the disk, because a defined edge still exists. In fact, there are deeper “nulls” at the edge of the shim because the edge is sharper, but these ripples smooth out towards the center as illustrated in Figure 4.6.

If the disks were larger in diameter, they could have been measured more accurately because edge diffraction would be less of a problem. In order to confirm this theory, a larger shim was used and the edges were tapered in the same way. However, useful results were not attained because the edge of the disk started to interfere with the edge of the aperture stop so that instead of having a circular aperture with a shim in it, the aperture was becoming more like an annulus.

Another shape that was measured was a 76mm square piece of Rexolite 0.762mm thick which yields a phase shift of 50° . This measurement illustrates even more effects from sharp edges since the square excites even more energy propagating at larger angles from the initial direction of propagation. The results shown in Figure 4.7 clearly illustrate the effects from the sharp edges and corners of the square.

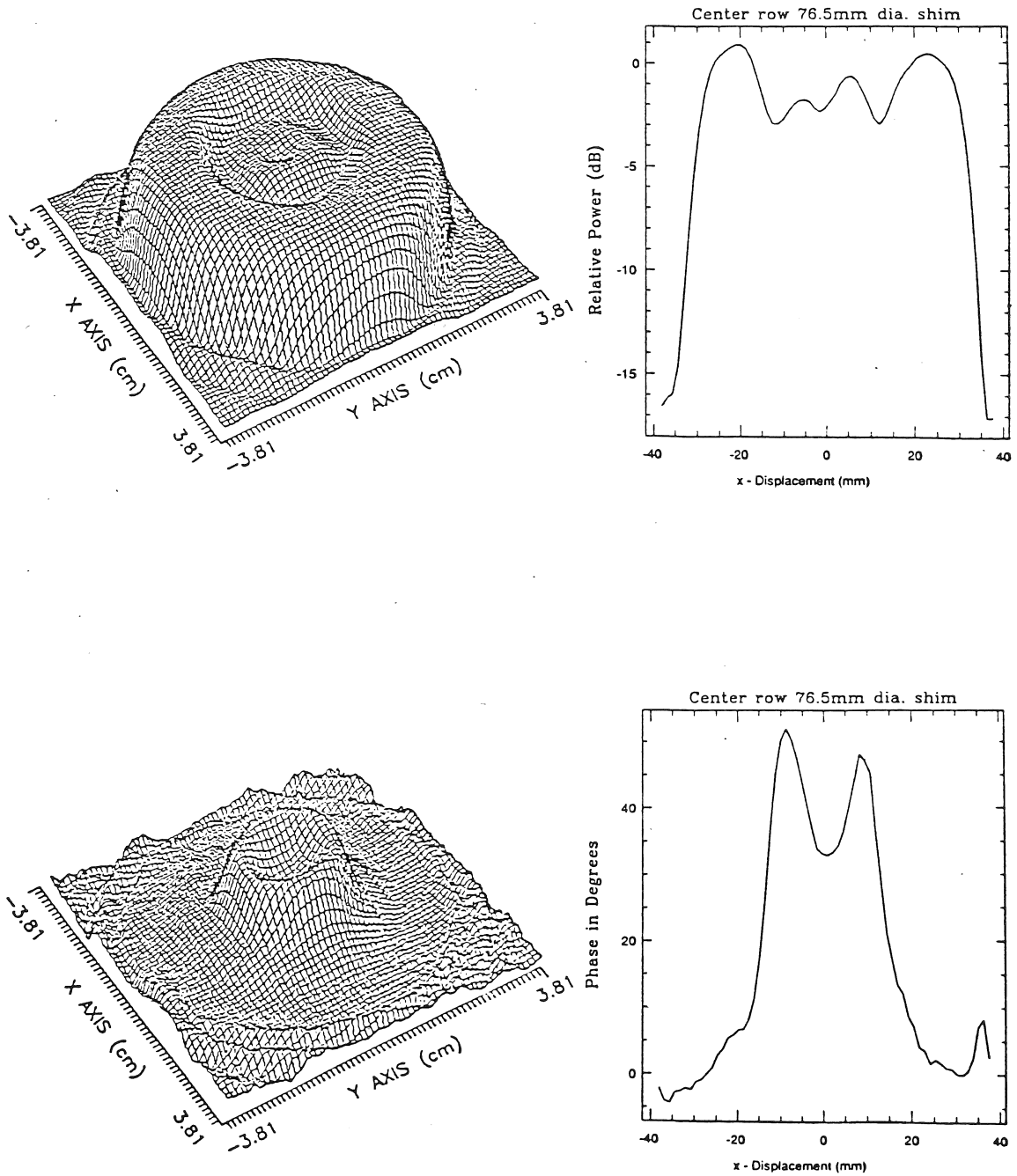
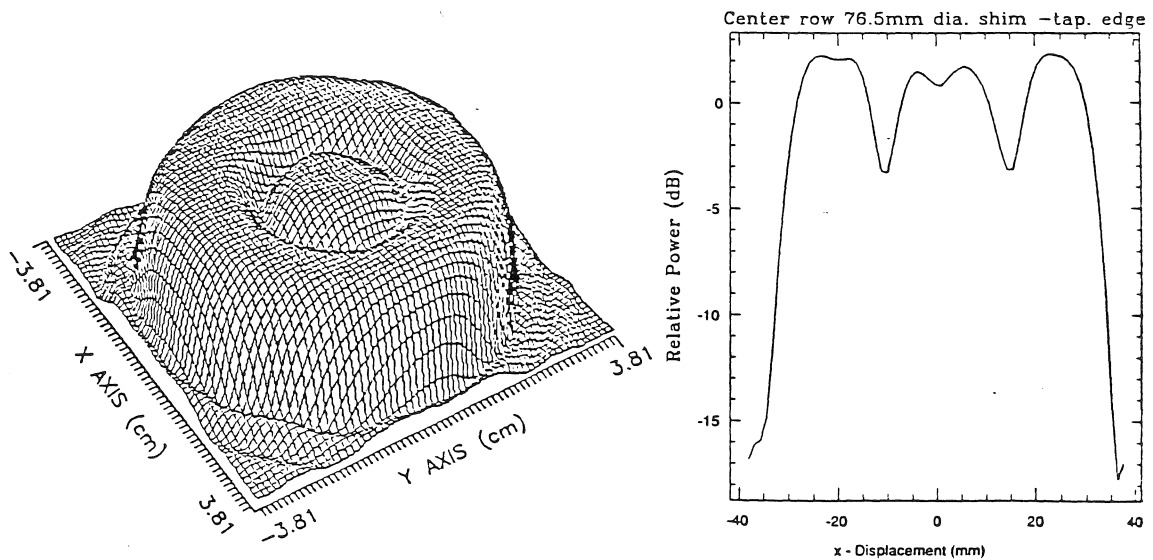
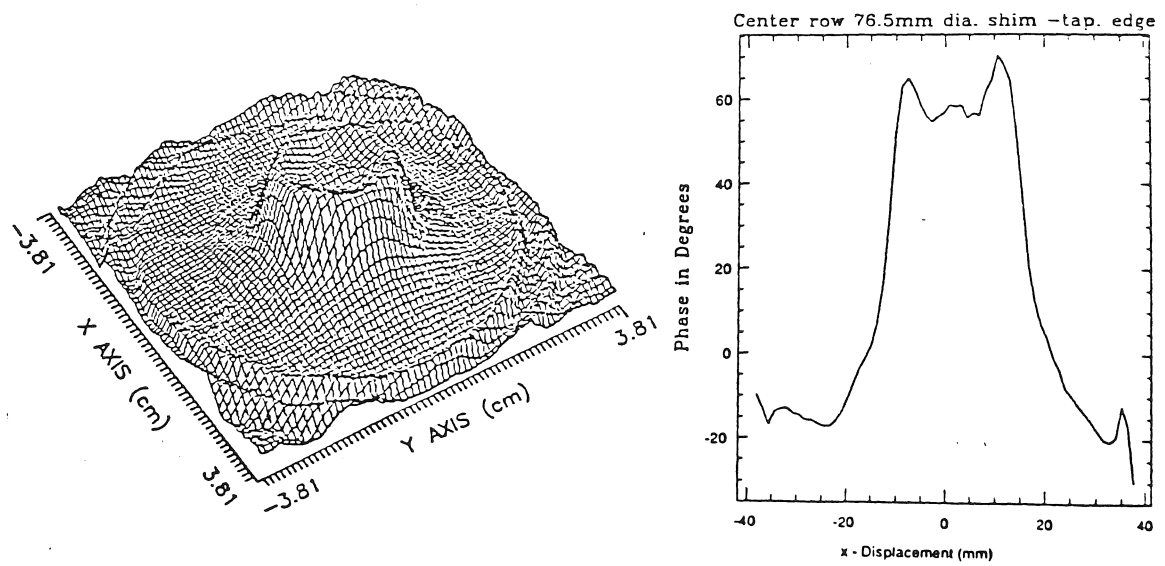


Figure 4.5 Amplitude (a) and phase (b) of the real image of a dielectric shim 76.2mm in diameter placed in the aperture plane of the objective lens. This shim is used to simulate a phase deviation of 50° .



(a)



(b)

Figure 4.6 Amplitude (a) and phase (b) of the real image of a dielectric shim 76.2mm in diameter with a tapered edge. The thickness of the shim produces a phase deviation of 78° .

Although the results show the effects from edge-diffraction, the phase of the shims were measured to within approximately 10° . Measuring to within this degree of accuracy implies that errors are being measured to within about $\frac{\lambda}{70}$. Measuring errors down to this level is quite adequate for removing large-scale or even small-scale errors in the main reflector of the antenna.

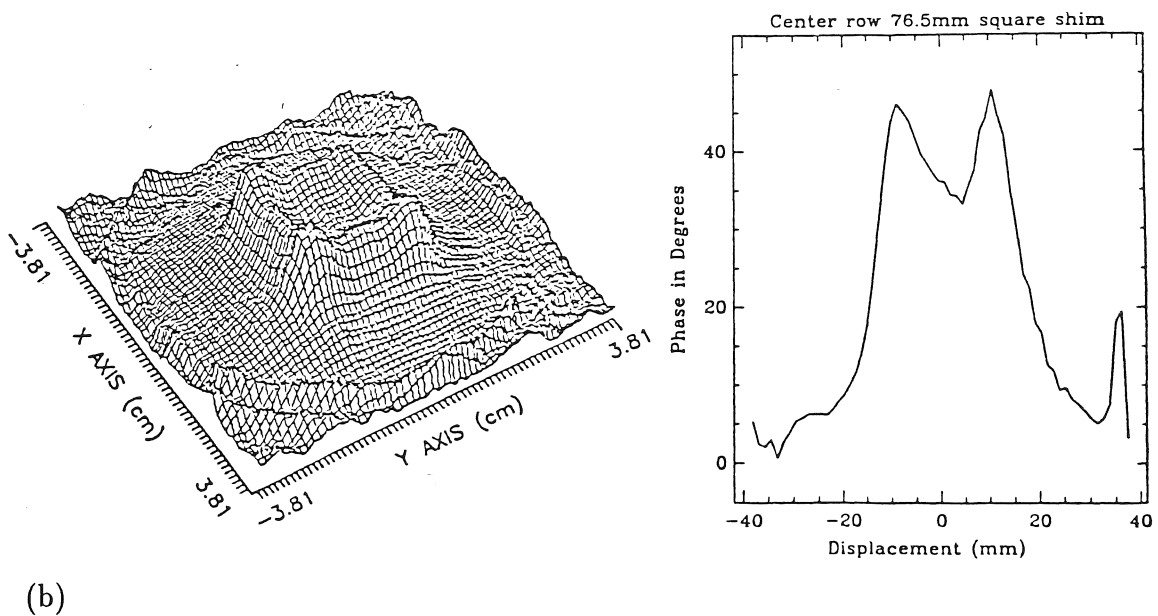
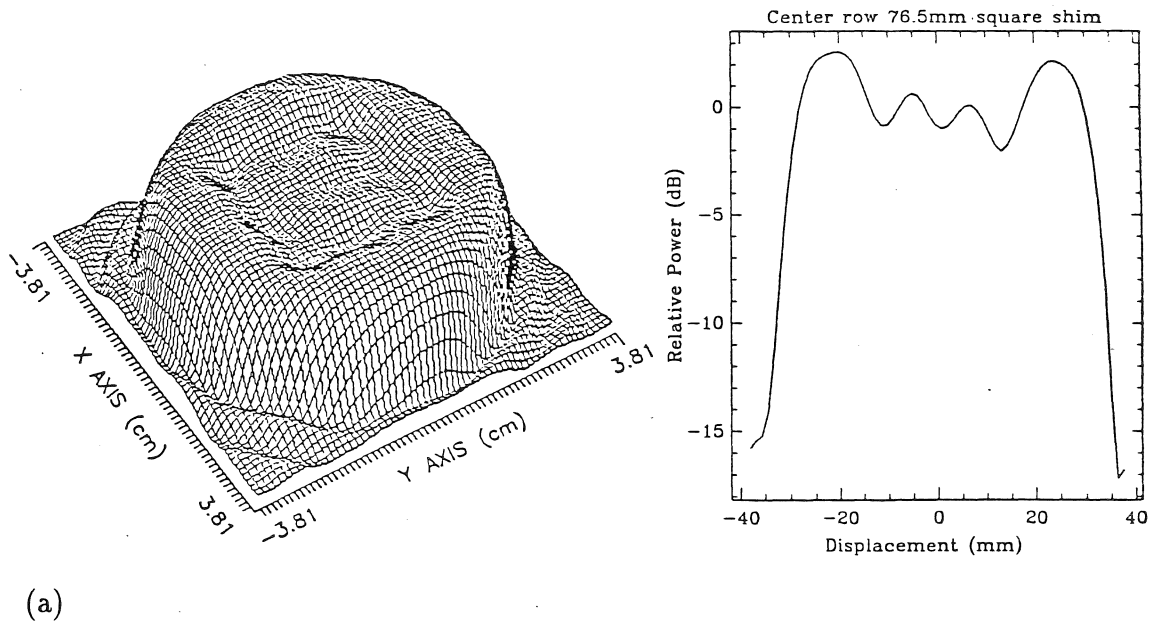


Figure 4.7 Amplitude (a) and phase (b) of the real image of a dielectric square 76.2mm in length. The thickness of the square should produce a phase perturbation of 50° .

CHAPTER 5

DISCUSSION

The results of this experiment illustrate some of the limitations in using the theory of Fourier optics for describing the imaging properties of the imaging system. Because of the longer wavelengths and smaller apertures used in the experiment, the effects of diffraction play too strong of a role and cannot be ignored. As a result, some of the approximations used to arrive at the results in Fourier optics at optical wavelengths are found not to be completely valid in millimeter wavelengths for the apertures used in this experiment. The strongest effects from diffraction are believed to come from edge effects of the aperture stop and the phase shims. The results from the measurements show that the theory of Fourier optics has problems in describing the effects from edge diffraction from the phase shims. It is suggested that a more rigorous calculation be performed at the different focal planes of the imaging system where the diffraction integrals are solved numerically in order to obtain more accurate results. However, this experiment was not the ideal situation to test the concept of imaging phase perturbations from the incident aperture plane. Because of the optics used, this experiment was restricted to measuring small scale errors. The goal of this approach was not intended to measure small scale deviations in the aperture plane, but to measure large scale perturbations

that would mainly arise from the gravitational deformation of the main reflector of the antenna. The perturbations measured in this experiment are only about 30 wavelengths in size whereas for large apertures, these errors are far from being large scale. Large scale errors would be on the order of at least several hundred wavelengths in size. Although the effects of edge diffraction for the large scale errors would be the same as for the small scale errors, the ripples produced from edge diffraction would smooth out over the larger surface area of the large scale perturbation. As for the case of the gravitational deformation of large reflector antennas, edge effects should be even less of a problem since the boundaries of these errors are very smooth and the overall size of the errors would be extremely large as compared to a wavelength. These smooth errors should not introduce any problems with edge diffraction. Edge effects ought to be less of a problem for larger apertures. However, it must be pointed out that as the diameter of the aperture increases, so does the distance to the Fresnel region. If the focal length of the antenna is not long enough to be in the Fresnel region, the principles of Fourier optics cannot be applied. This is because the phase term in the exponent of the Rayleigh–Sommerfeld diffraction formula cannot be approximated by using the binomial expansion theorem and therefore, the diffraction integral has to be solved numerically.

If the electric field is observed in the near-field region of the aperture, it is found that the edge taper will drop off faster for a large aperture than for a small aperture. This may be inferred by calculating the aperture distribution of the electric field in the near-field region by solving the diffraction integral numerically. Be-

cause of diffraction from the edge of the aperture, more attention is required in the approximations that lead to the Fourier transforming properties of lenses –namely the approximation to take into account the finite size aperture of the lens and how the electric field changes between the incident aperture plane and the front surface of the lens. Calculations using diffraction theory have shown that the electric field incident on the objective lens is not the same as in the incident aperture plane. If it were, the edge-taper of the electric field would be the same on the surface of the objective lens as it is in the aperture plane. Figure 5.1 illustrates the amplitude of the electric field for an aperture 76.2mm in diameter 304.8mm behind the aperture. This calculation was derived from a computer program which solves the Rayleigh–Sommerfeld diffraction theorem numerically. Theoretically, this would be the amplitude distribution incident on the objective lens of the imaging system. If the electric field were the same in the aperture plane as that incident to the objective lens, the electric field would essentially drop to zero for any distance greater than the radius of the aperture stop on the front surface of the lens. However, because of diffraction, the electric field does not drop to zero as the radius from the optical axis becomes greater than the radius of the aperture. For smaller wavelengths and for larger apertures, the approximation of the electric field dropping to zero at the edge of the lens becomes more valid. Figure 5.2 illustrates a comparison for a wavelength one tenth ($\frac{\lambda}{10}=0.3327\text{mm}$) that used in the experiment for the same distance behind the aperture. This result shows that the electric field for the smaller wavelength drops faster than for the wavelength used in the experiment. However, for the case of the shorter wavelength, the observation plane is not within

the Fresnel region.¹ It is not known how strict the condition of the Fresnel approximation in order for the higher terms in the binomial expansion to have a negligible contribution. In order to see how strict this condition is, a comparison between solving the diffraction integral using the Fresnel approximation and solving the diffraction integral numerically would be suggested. In either case, it is found that the lens has to be larger in diameter than the aperture stop in order to reduce truncation effects from the edge of the lens. The projection of the pupil function onto the aperture plane implies that the aperture distribution in the aperture plane is bounded, and the diameter of the lens now infinite. As a result of these calculations, for the diameter of the objective lens two times the diameter of the 150mm diameter aperture stop, the edge taper at the edge of the objective lens was found to be greater than 20 dB. With this edge taper, truncation of the electric field from the objective lens and the effects from edge diffraction are, however, small as was demonstrated in figure 4.4.

The measurements taken in this experiment illustrate truncation and edge effects from the optics used in reimaging the incident aperture distribution corrupted by phase errors. The principles of Fourier optics have problems in describing these effects. As a result, it is suggested that the diffraction integrals should be solved numerically to take the effects of edge diffraction into account. The results from this experiment are not conclusive in determining the feasibility of this approach because of the relatively small diameter of the optics used, and the phase errors

¹For the case of λ (3.327mm), the distance to the Fresnel zone is found to be 200mm, and for $\frac{\lambda}{10}$, 430mm. The objective lens has a focal length of 302mm and is therefore not in the Fresnel zone for the case of $\frac{\lambda}{10}$.

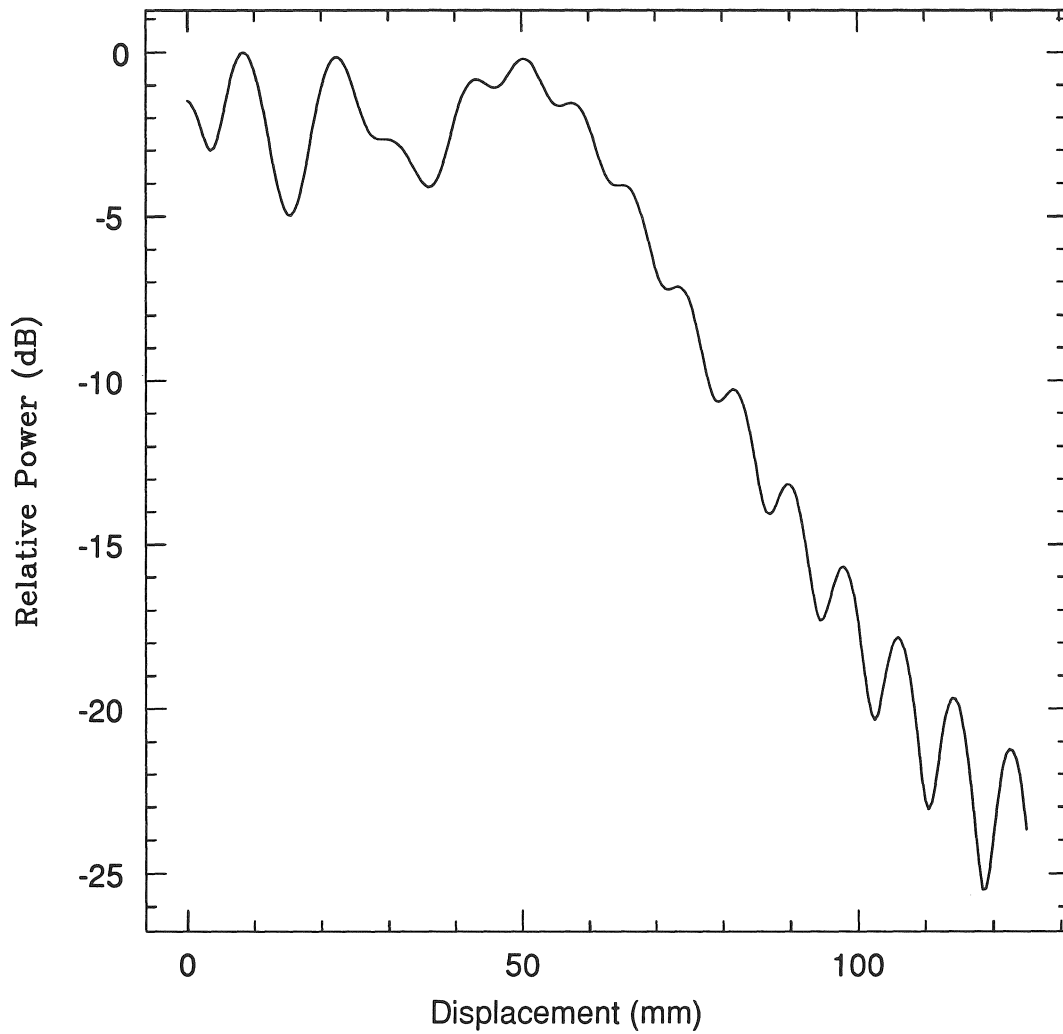


Figure 5.1 Calculated amplitude of the electric field incident on the lens for an aperture stop 76mm in diameter at a distance of 304.8mm behind the lens.

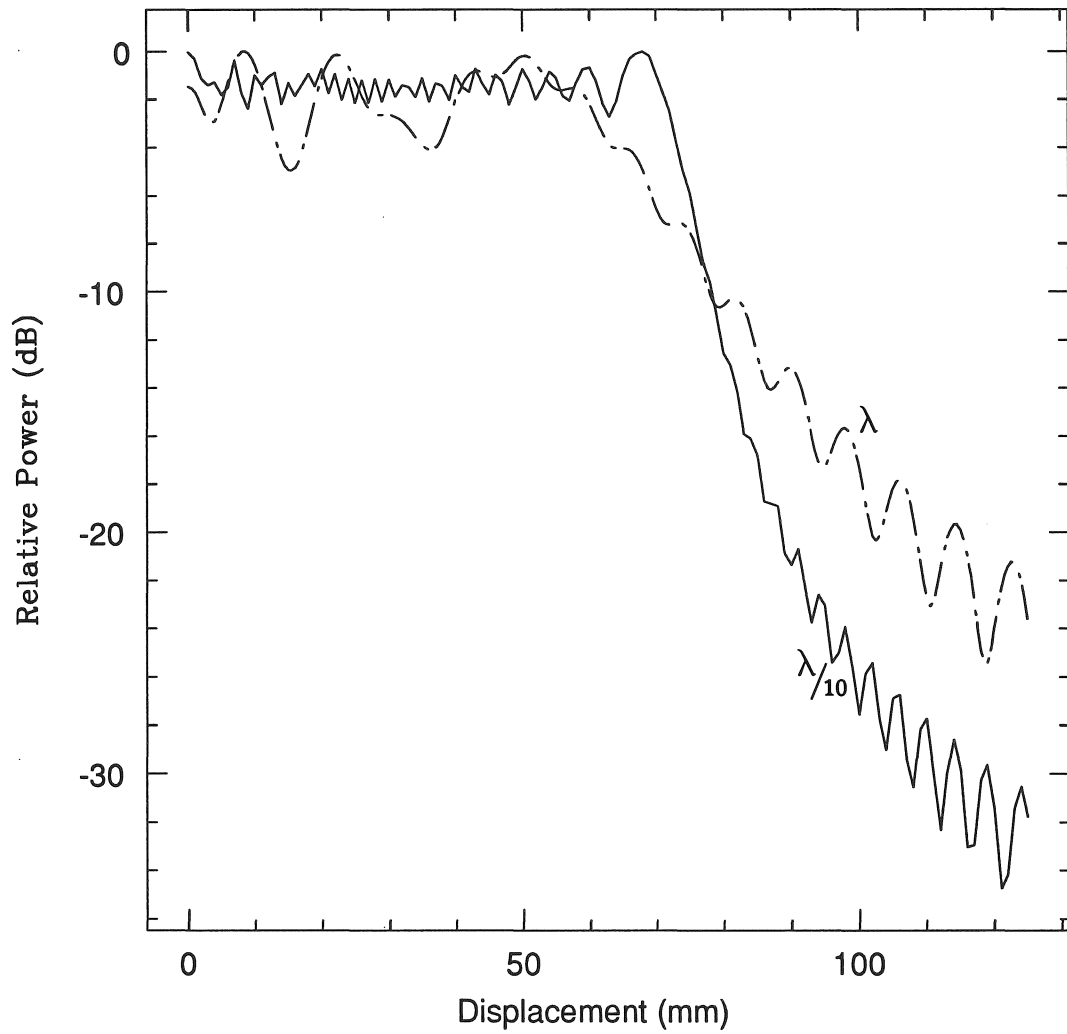


Figure 5.2 Comparison of the calculated electric field distribution incident on the objective lens between λ and $\lambda/10$.

with respect to wavelength are small-scale. The effects from diffraction imply that the errors cannot be scaled with wavelength. It is suggested that the same measurements be performed with larger diameter optics where larger-scale errors can be measured and edge-effects ought to be less troublesome. However, even with all of the errors discussed here, measuring phase errors to within 10° , as was done in this experiment, implies a RMS surface error of $\frac{\lambda}{72}$ at a wavelength of 3mm. This degree of accuracy is quite adequate for removing large-scale (or even small-scale) errors of the main reflector of the antenna.

CHAPTER 6

CONCLUSION

This experiment has investigated reimaging the incident aperture distribution to measure phase perturbations that may exist in the aperture plane. The basic approach in trying to understand how the incident aperture field is reimaged onto the image plane is through the principles of Fourier optics. A quasioptical imaging system was constructed and measurements were taken in an attempt to form images of phase perturbations placed in the aperture plane of the system. Using the principles of Fourier optics, a real image of the phase perturbations will be formed at the image plane of the imaging system. It was found that the theory of Fourier optics had limitations in describing the effects of diffraction from edges. Edge diffraction is found to cause interference in the electric field which causes ripples in the amplitude of the image of the phase shim. This ripple effect in amplitude should not exist for a perturbation that only affects phase. This ripple results in errors in the measurement of the phase at the boundary between the perturbation and free-space. This implies that the measurement of phase errors cannot be scaled with wavelength. In order to take these effects into consideration, a more rigorous calculation involving a more direct solution of the diffraction integrals would be required. This would imply that the diffraction integrals would have to

be solved numerically. The effects of edge diffraction would, therefore, adversely affect the accuracy in measuring small-scale perturbations. However, the phase of the perturbations measured in the image plane was in most cases, measured to within 10° . This degree of accuracy is more than adequate for correcting large-scale (or even small-scale) phase errors in the main reflector of a reflector antenna.

A P P E N D I X

FOURIER OPTICS

A.1 Scalar Diffraction Theory

Many theorems that exist in the development of scalar diffraction theory share the same origin. That is, most situations are boundary value problems whose solutions satisfy the Helmholtz wave equation. The fundamental mathematical tool for solving this type of problem is Green's theorem which may be stated as follows: For a continuous function U and Green's function G that exists over a volume V ,

$$\iiint_V \{G \nabla^2 U - U \nabla^2 G\} dV = \iint_S \left\{ G \frac{\partial U}{\partial n} - U \frac{\partial G}{\partial n} \right\} dS \quad (\text{A.1})$$

where $\frac{\partial F}{\partial n}$ implies $\nabla F \cdot \hat{n}$. This solution satisfies the Helmholtz wave equation in a homogeneous source-free medium with propagation constant $k = \frac{2\pi}{\lambda}$ for both the Green's function and the disturbance function:

$$(\nabla^2 + k^2)G = (\nabla^2 + k^2)U = 0. \quad (\text{A.2})$$

Green's theorem allows the boundary problem to be solved for which both the Green's function G , and the disturbance function U , satisfy the Helmholtz wave equation. The Green's function serves a dual purpose: it satisfies the boundary conditions of the given problem, and acts as the propagating function for the electromagnetic disturbance U , observed from some observation point originating from a boundary or surface S .

To illustrate how Green's theorem is used to develop a diffraction theorem, we start with a fundamental boundary problem of expressing the amplitude of an electromagnetic disturbance at an observation point O_p originating from some surface boundary S , which encloses the volume V surrounding O_p as illustrated in Figure A.1. The goal of the problem is to derive an expression for the electromagnetic disturbance at O_p in terms of the electromagnetic disturbance originating from the surface S .

Since the electromagnetic disturbance is a wave phenomenon it must satisfy the wave equation. Therefore, in order to describe the disturbance at O_p , the Helmholtz wave equation is used in conjunction with the application of Green's theorem. With the proper choice of a Green's function, a solution to the boundary value problem can be formulated. The resulting expression gives the observed electromagnetic disturbance at O_p in terms of the electromagnetic disturbance originating from the surface S . The disturbance seen at O_p can be described as the result of the sum of the contribution of point sources emitting spherical waves from the surface S . Therefore, a Green's function which describes a spherical wave propagating from a point source on the surface S is chosen. i.e.,

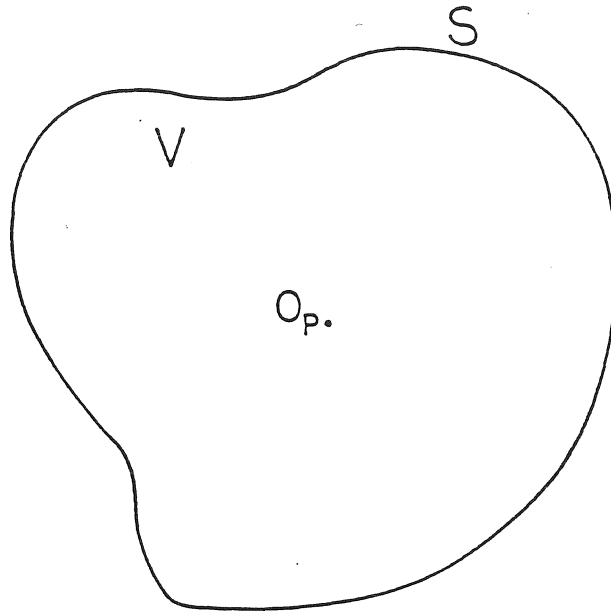
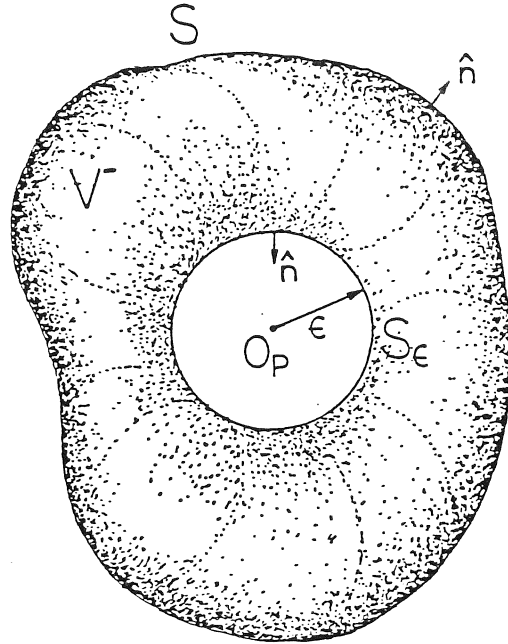


Figure A.1 Surface used to describe the development of a diffraction theorem by using Green's theorem.

$$G(P_1) = \frac{e^{jk r_{01}}}{r_{01}}. \quad (\text{A.3})$$

P_1 is an arbitrary point on S with r_{01} representing the distance from the observation point O_p to P_1 .

Before applying Green's theorem, note that a problem exists in using the chosen Green's function which occurs at the observation point O_p . A discontinuity exists here since $r_{01} \rightarrow 0$. In order to circumvent this discontinuity, a new surface S' is adopted. This surface as described in Figure A.2, and is similar to S except for a small spherical surface S_ϵ of radius ϵ surrounding the observation point P_0 . S' is the combined sum of the surfaces S and S_ϵ . That is,



$$S' = S + S_\epsilon$$

Figure A.2 Surface used to account for the point discontinuity from the observation point in observing the electric field.

$$S' = S + S_\epsilon \quad (\text{A.4})$$

Note that \hat{n} always points outward from the surface S' . Green's theorem may now be applied to the surface S' and volume V' . Both the disturbance function U , and the Green's function G , satisfy the Helmholtz wave equation. Applying Green's theorem to a source-free homogeneous volume,

$$\iiint_V \{G \nabla^2 U - U \nabla^2 G\} dV - \iint_{S'} \left\{ G \frac{\partial U}{\partial n} - U \frac{\partial G}{\partial n} \right\} dS' \equiv 0.$$

Using the Helmholtz wave equation,

$$\nabla^2 U = -k^2 U ; \quad \nabla^2 G = -k^2 G$$

The preceding expression may be rewritten as,

$$\iiint_V \{G U k^2 - U k^2 G\} dV = \iint_{S'} \left\{ G \frac{\partial U}{\partial n} - U \frac{\partial G}{\partial n} \right\} dS' = 0.$$

Decomposing S' ,

$$\begin{aligned} \iint_{S'} \left\{ G \frac{\partial U}{\partial n} - U \frac{\partial G}{\partial n} \right\} dS' &= \iint_{S_\epsilon} \left\{ G \frac{\partial U}{\partial n} - U \frac{\partial G}{\partial n} \right\} dS_\epsilon + \iint_S \left\{ G \frac{\partial U}{\partial n} - U \frac{\partial G}{\partial n} \right\} \\ &= 0 \end{aligned}$$

$$-\iint_{S_\epsilon} \left\{ G \frac{\partial U}{\partial n} - U \frac{\partial G}{\partial n} \right\} dS_\epsilon = \iint_S \left\{ \frac{\partial U}{\partial n} - U \frac{\partial G}{\partial n} \right\} dS. \quad (\text{A.5})$$

Using the defined Green's function for a general point P_1 on the surface of S_ϵ ,

$$G(P_1) = \frac{e^{jk r_{01}}}{r_{01}} ; \quad \partial_n G(P_1) \Rightarrow \nabla G(P_1) \cdot \hat{n}$$

$$\nabla G(P_1) = \frac{e^{jk r_{01}}}{r_{01}} \left(jk - \frac{1}{r_{01}} \right) (r_{01} \hat{r} \cdot \hat{n})$$

Since the magnitude of the unit vectors \hat{r}_{01} and \hat{n} are unity, $\hat{r}_{01} \cdot \hat{n}$ is just the cosine of the angle between \hat{r}_{01} and \hat{n} . On S , $\hat{r}_{01} \cdot \hat{n} = 1$, and on S_ϵ $\hat{r}_{01} \cdot \hat{n} = -1$. As a result, the expression for Green's theorem becomes

$$\begin{aligned} &-\iint_{S_\epsilon} \left\{ \frac{e^{jk r_{01}}}{r_{01}} \left[\frac{\partial U(P_1)}{\partial n} \right] + U(P_1) \left[\frac{e^{jk \epsilon}}{\epsilon} \left(jk - \frac{1}{\epsilon} \right) \right] \right\} dS_\epsilon \\ &= \iint_S \left\{ \frac{e^{jk r_{01}}}{r_{01}} \left[\frac{\partial U}{\partial n} \right] - U \frac{\partial}{\partial n} \left[\frac{e^{jk r_{01}}}{r_{01}} \right] \right\} dS. \end{aligned} \quad (\text{A.6})$$

With $dS_\epsilon = \epsilon^2 \sin \theta d\theta d\phi$ and the limits of $S_\epsilon \rightarrow \int_0^{2\pi} \int_0^\pi$, the integral on the left side of eq. (A.6) becomes

$$\begin{aligned}
& - \int_0^{2\pi} \int_0^\pi \left\{ G(P_1) \frac{\partial U(P_1)}{\partial n} + U(P_1) \left[\frac{e^{jk\epsilon}}{\epsilon} \left(jk - \frac{1}{\epsilon} \right) \right] \right\} \epsilon^2 \sin \theta d\theta d\phi \\
& = -2\pi \left\{ G(P_1) \frac{\partial U(P_1)}{\partial n} + U(P_1) \left[\frac{e^{jk\epsilon}}{\epsilon} \left(jk - \frac{1}{\epsilon} \right) \right] \right\} \epsilon^2 \cos \theta \Big|_0^\pi \\
& = 4\pi \left\{ G(P_1) \frac{\partial U(P_1)}{\partial n} + U(P_1) \left[\frac{e^{jk\epsilon}}{\epsilon} \left(jk - \frac{1}{\epsilon} \right) \right] \right\} \epsilon^2
\end{aligned}$$

taking the limit as $\epsilon \rightarrow 0$,

$$4\pi \epsilon^2 \left\{ G(P_o) \frac{\partial U(P_o)}{\partial n} + U(P_o) \left[\frac{e^{jk\epsilon}}{\epsilon} \left(jk - \frac{1}{\epsilon} \right) \right] \right\}_{\epsilon \rightarrow 0} = 4\pi U(P_o). \quad (\text{A.7})$$

This is the sought after expression for the electromagnetic disturbance observed at the observation point O_p . The disturbance seen at O_p may now be expressed in terms of the disturbance arising from the surface S' as

$$U(P_o) = \frac{1}{4\pi} \iint_{S'} \left\{ \frac{e^{jkr_{o1}}}{r_{o1}} \left[\frac{\partial U}{\partial n} \right] - U \frac{\partial}{\partial n} \left[\frac{e^{jkr_{o1}}}{r_{o1}} \right] \right\} dS'. \quad (\text{A.8})$$

This result is known as the Helmholtz–Kirchoff integral theorem [8], and is one of the fundamental integral theorems in scalar diffraction theory. This diffraction theorem allows the field at the point P_o to be expressed in terms of the wave disturbance on the surface (or boundary) enclosing the observation point.

A.2 The Rayleigh–Sommerfeld diffraction theorem

By applying Green's theorem, a general diffraction theorem can be derived through solving a specific boundary value problem by choosing an appropriate Green's function. The solution to this problem is by no means unique. Any number of diffraction formulas may be derived from a boundary value problem by applying different Green's functions. As a result, a particular boundary value problem may have many solutions. A specific problem is solved in such a manner as to choose the appropriate boundary conditions and Green's function to allow for a unique solution. The Rayleigh–Sommerfeld diffraction theorem is the direct result of the choice of a specific Green's function which satisfies a specific boundary value problem. The solution to this problem is one that is very useful in the analysis of lenses and apertures.

In order to observe an electromagnetic disturbance at the observation point O_p behind the screen as described in Figure A.3, a particular Green's function found by Sommerfeld [8], may be chosen which satisfies the boundary conditions of the problem and will yield a useful result in solving diffraction problems involving lenses. This Green's function implies that either G or $\partial G/\partial n$ vanishes over the entire surface of the screen S_a . This eliminates an inconsistency in applying the more restrictive set Kirchoff boundary conditions to the screen where the disturbance function U and its derivative must be identically zero everywhere on the screen except where the aperture exists. Since the Green's function found by Sommerfeld implies that the electric field is zero over the opaque part of the screen, the wave equation now has a solution which vanishes over the entire screen. This

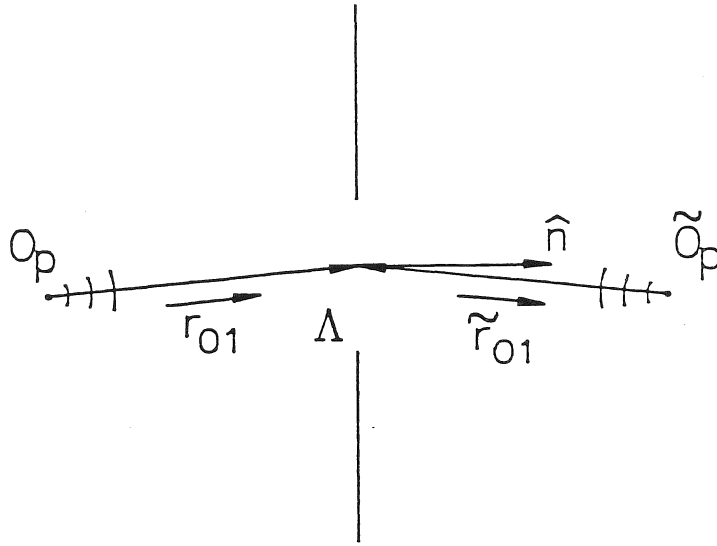


Figure A.3 Screen and point sources used to derive the Rayleigh-Sommerfeld diffraction theorem.

result implies that the Green's function must vanish over all space. Therefore, the boundary conditions on the disturbance function U are removed. This cannot be done using the Kirchoff boundary conditions where the boundary conditions have to be applied to both the Green's function G and the disturbance function U . (A more detailed discussion on the Kirchoff boundary conditions may be found in [8] and [9].)

The Rayleigh-Sommerfeld diffraction theorem is derived by solving the boundary value problem illustrated in Figure A.3. Both sources are coherent, and are oscillating at 180° with respect to each other (they may also be in phase). The Green's function chosen by Sommerfeld defined in the aperture of the screen may be written as

$$G_- = \frac{e^{jk r_{01}}}{r_{01}} - \frac{e^{jk \tilde{r}_{01}}}{\tilde{r}_{01}}. \quad (\text{A.9})$$

Then we find

$$\frac{\partial G_-(P_1)}{\partial n} = (\hat{n} \cdot \hat{r}_{01}) \left(jk - \frac{1}{r_{01}} \right) \frac{e^{jk r_{01}}}{r_{01}} - (\hat{n} \cdot \tilde{r}_{01}) \left(jk - \frac{1}{\tilde{r}_{01}} \right) \frac{e^{jk \tilde{r}_{01}}}{\tilde{r}_{01}}$$

where

$$|\vec{r}_{01}| = |\tilde{r}_{01}| \text{ and } \hat{n} \cdot \hat{r}_{01} = -\hat{n} \cdot \hat{\tilde{r}}_{01}.$$

Therefore,

$$\frac{\partial G_-(P_1)}{\partial n} = 2(\hat{n} \cdot \hat{r}_{01}) \left(jk - \frac{1}{r_{01}} \right) \frac{e^{jk r_{01}}}{r_{01}}.$$

Substituting $G_-(P_1)$ into the Helmholtz–Kirchoff integral theorem, one obtains the following result (assuming that $r_{01} \gg 1$):

$$\begin{aligned} U(P_o) &= \frac{1}{4\pi} \int_S \left[G_-\left(\frac{\partial U}{\partial n}\right) - U\left(\frac{\partial G_-}{\partial n}\right) \right] dS \\ &= \frac{1}{4\pi} \int_S \left[\frac{\partial U}{\partial n} - 2U(P_1) \left(\hat{n} \cdot \hat{r}_{01} \frac{e^{jk r_{01}}}{r_{01}} \right) \right] dS \\ &= \frac{1}{4\pi} \int_S \left[U(P_1) 2 \left(\frac{j2\pi}{\lambda r_{01}} - \frac{1}{r_{01}} \right) e^{jk r_{01}} (\hat{n} \cdot \hat{r}_{01}) \right] dS \end{aligned}$$

This finally gives, the Rayleigh–Sommerfeld diffraction theorem:

$$U(P_o) \simeq \frac{1}{j\lambda} \int_{\Lambda} \left[U(P_1) \frac{e^{jk r_{01}}}{r_{01}} (\hat{n} \cdot \hat{r}_{01}) \right] dS. \quad (\text{A.10})$$

Where Λ is the surface of the gap in the screen. Eq. (4.10) expresses the electromagnetic disturbance seen at the observation point O_p in terms of the electromagnetic disturbance seen at the screen. Notice how the Green's function is in the form of a propagating wave. This implies that the Green's function acts as the propagating function for the electromagnetic disturbance on the aperture plane. Another observation is that the boundary conditions may now be applied to U alone and not on $\partial U/\partial n$. This extra degree of freedom thus eliminates the inconsistencies implied from the Kirchoff boundary conditions [8]. Eq. (4.10) is known as the Rayleigh–Sommerfeld diffraction theorem and is that which is applied in this thesis.

A.2.1 The Sommerfeld Radiation Condition

The Green's function found by Sommerfeld solves the problems encountered in trying to express the electric field on the surface of the screen described in figure A.4. Applying this Green's function, the electric field on the surface S_a is found to be zero, and the wave equation now has a solution over the surface of the entire screen, and the boundary conditions on the disturbance function U are removed. Another issue that must be addressed is the electromagnetic distribution over the surface S_b . Since we are only interested in the aperture distribution over the screen, we must somehow detach the aperture distribution over the screen from the surface S_b . This problem has been solved by Sommerfeld, and is described as follows:

On the surface S_b the Green's function may be written as

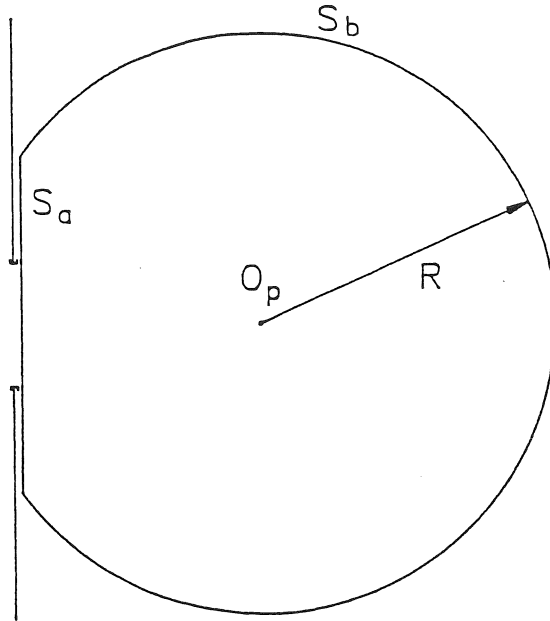


Figure A.4 Surface used in describing the Sommerfeld radiation condition.

$$G = \frac{e^{(jkR)}}{R} \frac{\partial G}{\partial n} = \left(jk - \frac{1}{R} \right) \frac{e^{(jkR)}}{R} \simeq jkG. \quad (\text{A.11})$$

The last approximation is justified for large R . Applying Green's theorem we obtain

$$\iint_{S_b} \left[G \frac{\partial U}{\partial n} - U(jkG) \right] dS = \int_{\Omega} GR^2 \left(\frac{\partial U}{\partial n} - jkU \right) d\Omega. \quad (\text{A.12})$$

As R increases to infinity, the above integral will vanish if

$$\lim_{R \rightarrow \infty} R \left(\frac{\partial U}{\partial n} - jkU \right) = 0. \quad (\text{A.13})$$

This condition is known as the Sommerfeld radiation condition. If U diverges at least as fast as a spherical wave, the Sommerfeld radiation condition will be satisfied. Therefore, if U is represented as a spherical wave,

$$U = \frac{e^{jkR}}{R}$$

$$\frac{\partial U}{\partial n} = \left(jk - \frac{1}{R} \right) \frac{e^{jkR}}{R}$$

$$\simeq jkU$$

$$\begin{aligned} \lim_{R \rightarrow \infty} R \left(\frac{\partial U}{\partial n} - jkU \right) &= Rjk(U - U) \\ &= 0. \end{aligned}$$

A.3 The Fresnel and Fraunhofer approximations

Having derived the Rayleigh–Sommerfeld diffraction formula, we are now in a position to solve certain boundary value problems. However, certain mathematical approximations must be made to facilitate the diffraction calculations. If an exact solution is desired, direct solutions may be obtained by using a computer. In addition to facilitating a direct calculation of the diffraction pattern, the approximations allow the reader to obtain a deeper understanding of the results without getting bogged down with mathematical details.

To begin, the Rayleigh–Sommerfeld diffraction formula may be rewritten in a more descriptive form which illustrates the physical interpretation of each term of

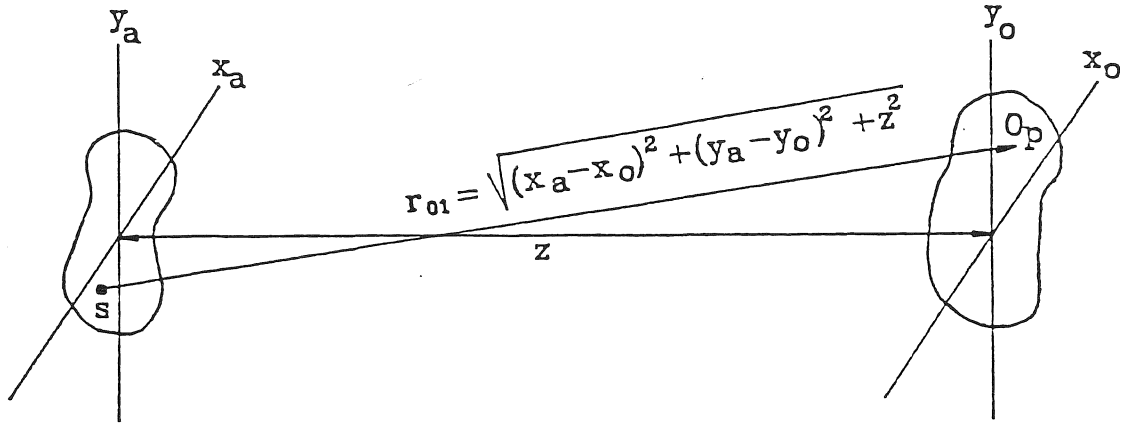


Figure A.5 Diffraction geometry for deriving the Fresnel and Fraunhofer approximations.

the expression. With reference to Figure A.5, the problem is set up in the following manner:

A point in the aperture plane is characterized by the coordinates (x_a, y_a) , and the observation plane by (x_o, y_o) and it is assumed that the distance from the aperture to the observation plane is much greater than λ . Recall that the Green's function was found to be the propagating function for the electromagnetic disturbance on the screen. It may be characterized as the transfer function of the aperture. With these definitions in mind, the Rayleigh-Sommerfeld diffraction formula may be written as

$$\begin{aligned}
 U(S) &= U(x_a, y_a) \text{ (Aperture plane)} \\
 U(O_p) &= U(x_o, y_o) \text{ (Observation plane)} \\
 h(S, O_p) &= h(x_o, y_o; x_a, y_a) = \frac{1}{j\lambda} \frac{e^{jk r_{01}}}{r_{01}} (\hat{n} \cdot \hat{r}_{01}).
 \end{aligned}$$

The somewhat awkward looking notation for the transfer function is written in order to illustrate the mapping or transfer from the aperture plane to the observation plane.

$$U(x_o, y_o) = \iint_{\Lambda} h(x_o, y_o; x_a, y_a) U(x_a, y_a) dx_a dy_a \quad (\text{A.14})$$

The first approximation is that the electromagnetic disturbance only exists in the aperture so that the limits of integration may be expanded from Λ to $\pm\infty$. The second and more involved approximation involves the vector term r_{01} in both the exponent and in the denominator of the integrand. With reference to Figure A.5, with the distance between the aperture and the screen being much greater than λ , $\hat{n} \cdot \hat{r}_{01}$ (sometimes called the “obliquity factor”) may be approximated to unity. r_{01} in the denominator can be approximated as being equal to z . However, such a simple approximation cannot be made for the term in the exponent for the transfer function. This is because of the relatively large magnitude of the propagation constant k which could consequently generate phase errors greater than 2π radians. The distance r_{01} may be written as

$$\begin{aligned} r_{01} &= \sqrt{(x_0 - x_a)^2 + (y_0 - y_a)^2 + z^2} \\ &= z \sqrt{1 + \left(\frac{x_0 - x_a}{z}\right)^2 + \left(\frac{y_0 - y_a}{z}\right)^2} \end{aligned} \quad (\text{A.15})$$

r_{01} , may be approximated by performing a binomial expansion on the square root. Expanding out to a first-order approximation we find

$$r_{01} \simeq z \cdot \left[1 + \frac{1}{2} \left(\frac{x_0 - x_a}{z}\right)^2 + \frac{1}{2} \left(\frac{y_0 - y_a}{z}\right)^2 \right] \quad (\text{A.16})$$

The preceding approximation is sometimes referred to as the *Fresnel approximation*, which was made with the restriction that the next higher order phase term in the binomial expansion for r_{01} is in the exponent is less than 1 radian. This condition is satisfied as long as

$$z \gg \sqrt[3]{\frac{\pi}{4\lambda} [(x_0 - x_a)^2 + (y_0 - y_a)^2]^2} \quad (\text{A.17})$$

or for an aperture of diameter D ,

$$z \gg \sqrt[3]{\frac{\pi D^4}{64\lambda}}. \quad (\text{A.18})$$

This condition must be applied with caution. It is not known how strict this condition is in order for the higher order terms to have a negligible contribution. The region for which z satisfies the Fresnel approximation is known as the Fresnel region. However, the higher order terms must have an negligible contribution in order to derive the theory of Fourier optics.

With the new approximation made for r_{01} , the transfer or weighting function may be written as

$$h(x_o, y_o; x_a, y_a) = \frac{e^{jkz}}{j\lambda z} e^{j\frac{k}{2z} [(x_o - x_a)^2 + (y_o - y_a)^2]}$$

Therefore, the diffraction pattern seen at the observation plane $U(x_o, y_o)$, is given by

$$U(x_o, y_o) = \frac{e^{jkz}}{j\lambda z} \times \int \int_{-\infty}^{\infty} U_s(x_a, y_a) e^{j\frac{k}{2z}[(x_o-x_a)^2+(y_o-y_a)^2]} dx_a dy_a \quad (\text{A.19})$$

Examining this expression in more detail, $U(x_o, y_o)$ may be interpreted as the *convolution* of $U_s(x_o, y_o)$ with the transfer function $h(x_o, y_o)$. Pay close attention to the dummy variables. Note that the dummy variable for the source function changes from $U_s(x_a, y_a)$ to $U_s(x_o, y_o)$ and that this function is being convolved with $h(x_o, y_o)$ and not with $h(x_o - x_a, y_o - y_a)$!

$$U(x_o, y_o) = U_s(x_o, y_o) * h(x_o, y_o)$$

If the quadratic phase term in the exponent of the transfer function is expanded, the resulting expression resembles a Fourier transform relationship between the aperture plane distribution and the aperture distribution in the observation plane. The only difference is an extra quadratic phase term in front of the integral. The following expression is known as the *Fresnel* diffraction formula.

$$U(x_o, y_o) = \frac{e^{jkz}}{j\lambda z} e^{[j\frac{k}{2z}(x_o^2+y_o^2)]} \times \int \int_{-\infty}^{\infty} U(x_a, y_a) e^{j\frac{k}{2z}(x_a^2+y_a^2)} e^{-j\frac{2\pi}{\lambda z}(x_o x_a + y_o y_a)} dx_a dy_a \quad (\text{A.20})$$

If r_{01} is increased further, an even simpler expression may be obtained for the diffraction pattern seen at the observation plane. If z satisfies the relation

$$z \gg \frac{k(x_a^2 + x_0^2)}{2},$$

the quadratic phase term in the integrand disappears, and a direct Fourier transform relation exists between the aperture plane aperture distribution and the observation plane aperture distribution. This region is known as the *Fraunhofer* or *far-field* region. With this approximation, the diffraction pattern seen in the observation plane is given by

$$U(x_0, y_0) = \frac{e^{jkz} e^{j\frac{k}{2z}(x_0^2 + y_0^2)}}{\lambda z} \times \int_{-\infty}^{\infty} \int_{-\infty}^{\infty} U(x_a, y_a) e^{-j\frac{2\pi}{\lambda z}(x_0 x_a + y_0 y_a)} dx_a dy_a \quad (\text{A.21})$$

The relation between the aperture plane and the observed diffraction pattern in the Fraunhofer region is a direct Fourier transform relation except for a quadratic phase term which appears in front of the integral.

A.4 Derivation of the Fourier transforming property of lenses

From the study of scalar diffraction theory, it was found that the near-field or Fresnel region diffraction pattern is related to the Fourier transform of the incident aperture distribution except for a quadratic phase term in the integrand. This implies that the spherical waves emanating from each of the point sources on the aperture may be approximated by quadratic surfaces. A lens comprised of a

material in which the velocity of electromagnetic waves is different than that of air can be used to transform the quadratic surface wavelets into plane waves. This is accomplished by controlling the thickness of the lens in order to introduce the conjugate phase delay to convert the quadratic surface wavelets into plane waves. Mathematically, the lens cancels out the quadratic phase term in the integrand of the Fresnel region diffraction formula. This, simplifies the expression to a direct Fourier transform relationship between the aperture distribution of the electromagnetic field incident on the lens and the diffraction pattern generated at the focal plane of the lens. In effect, the lens places the source at infinity so that the diffraction pattern given at the focal plane of the lens is the far-field pattern of the aperture of the source.

A.4.1 *The lens thickness function*

A lens may effectively be called a progressive phase shifter. The term progressive is used because the thickness of the lens varies with position. Mathematically, the amount of phase delay experienced by the incident wavelet at position (x,y) , is given as follows (see Figure A.6)

$$\phi(x, y) = kn\tau(x, y) + k[\tau_0 - \tau(x, y)], \quad (\text{A.22})$$

where n is the index of refraction of the lens, τ_0 , the maximum thickness of the lens, $kn\tau$ the phase delay introduced by the lens, and $k[\tau_0 - \tau(x, y)]$, the phase delay of the remaining free-space between the two reference planes. With this convention, the added phase term may be written as

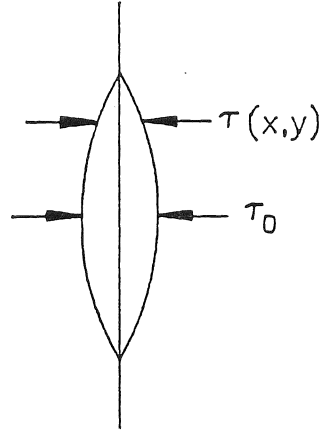


Figure A.6 Lens thickness cross-section.

$$e^{jkn\tau(x,y)}e^{jk[\tau_0-\tau(x,y)]} = e^{jk(n-1)\tau(x,y)}e^{jk\tau_0}. \quad (\text{A.23})$$

The transmittance function (the function which describes the propagation of electromagnetic waves through the lens), of the lens is simply the magnitude of the propagating wave through the lens which is taken to be unity, together with the phase shift introduced by the thickness function:

$$t(x, y) = \phi(x, y) = e^{jk\tau_0}e^{jk(n-1)\tau(x,y)}. \quad (\text{A.24})$$

The aperture distribution function on the back plane of the lens $U'_l(x, y)$ may be written as

$$U'_l(x, y) = t(x, y)U_l(x, y) = U_l(x, y)e^{jk\tau_0}e^{jk(n-1)\tau(x,y)} \quad (\text{A.25})$$

The thickness function of the lens may be defined more formally with respect to the surface geometry of the lens. But first, a sign convention must be adopted in order to act as a reference point for the radii of curvature of the lens. Therefore, the following sign convention is defined with reference to Figure A.6:

1. Rays travel from left to right.
2. Positive radius of curvature \Rightarrow convex surface to the incident rays.
3. Negative radius of curvature \Rightarrow concave surface to the incident rays.

The geometry of the thickness function of the lens may be expanded as

$$\tau(x, y) = \tau_1(x, y) + \tau_2(x, y) \quad (\text{A.26})$$

where τ_1 corresponds to the left half of the lens, and τ_2 corresponds to the right half of the lens.

$$\begin{aligned} \tau_1(x, y) &= \tau_{01}(x, y) - \left(R_1 - \sqrt{R_1^2 - x^2 - y^2} \right) \\ &= \tau_{01}(x, y) - R_1 \left(1 - \sqrt{1 - \frac{x^2 + y^2}{R_1^2}} \right) \end{aligned} \quad (\text{A.27})$$

$$\begin{aligned} \tau_2(x, y) &= \tau_{02}(x, y) - \left(-R_2 - \sqrt{R_2^2 - x^2 - y^2} \right) \\ &= \tau_{02}(x, y) + R_2 \left(1 - \sqrt{1 - \frac{x^2 + y^2}{R_2^2}} \right) \end{aligned} \quad (\text{A.28})$$

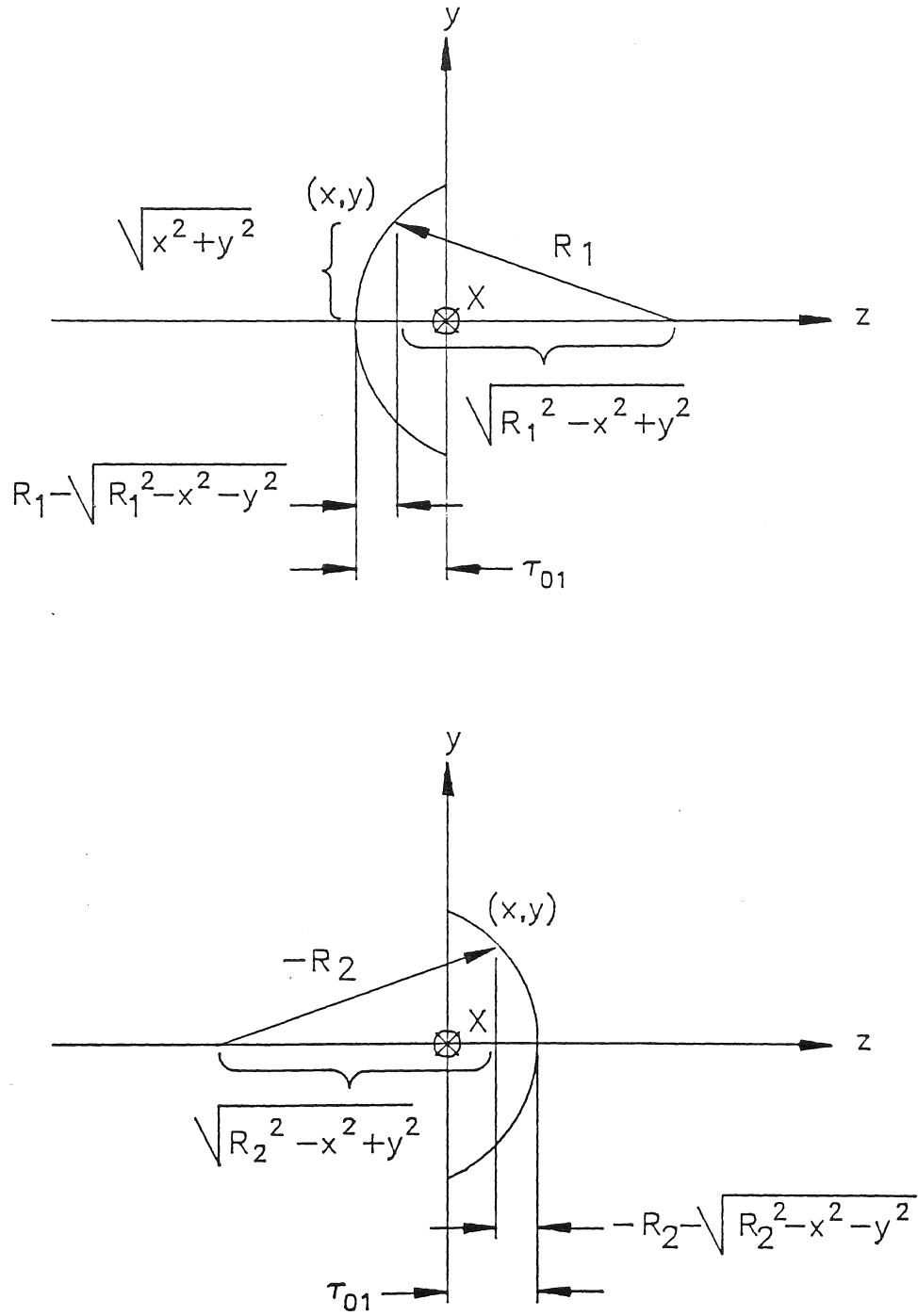


Figure A.7 Illustration of the thickness function of the lens in terms of the radius of curvature.

Therefore, the overall thickness function of the lens may be written as

$$\begin{aligned} \tau(x, y) &= \tau_{01}(x, y) + \tau_{02}(x, y) - \\ &R_1 \left(1 - \sqrt{1 - \frac{x^2 + y^2}{R_1^2}} \right) + R_2 \left(1 - \sqrt{1 - \frac{x^2 + y^2}{R_2^2}} \right) \end{aligned} \quad (\text{A.29})$$

If x and y are sufficiently small, the radical terms may be approximated by expanding the radical and taking only the lower order terms. This approximation is valid as long as the wavefront close to the optical axis is considered such that x and y are sufficiently small. (Be careful! If a large departure from the optical axis of the lens is to be considered, this approximation may no longer be valid. This is especially true if the radii of curvature of the lens are small). Therefore, the expressions in the radical may be approximated as

$$\sqrt{1 - \frac{x^2 + y^2}{R_1^2}} \simeq 1 - \frac{x^2 + y^2}{2R_1^2}$$

$$\sqrt{1 - \frac{x^2 + y^2}{R_2^2}} \simeq 1 - \frac{x^2 + y^2}{2R_2^2},$$

and the thickness function may now be written as

$$\begin{aligned} \tau(x, y) &= \tau_0 R_1 \left(1 - 1 + \frac{x^2 + y^2}{2R_1^2} \right) + R_2 \left(1 - 1 + \frac{x^2 + y^2}{2R_2^2} \right) \\ &= \tau_0 - \frac{x^2 + y^2}{2} \left(\frac{1}{R_1} - \frac{1}{R_2} \right). \end{aligned} \quad (\text{A.30})$$

With this result, the transmittance function may be written as

$$\begin{aligned}
t(x, y) &= e^{jk\tau_0} e^{jk(n-1)\left[\tau_0 - \frac{(x^2+y^2)}{2}\left(\frac{1}{R_1} - \frac{1}{R_2}\right)\right]} \\
&= e^{jkn\tau_0} e^{-jk(n-1)\left[\frac{(x^2+y^2)}{2}\left(\frac{1}{R_1} - \frac{1}{R_2}\right)\right]}.
\end{aligned} \tag{A.31}$$

The focal length is defined such that

$$\frac{1}{f} \equiv (n-1) \left[\frac{1}{R_1} - \frac{1}{R_2} \right] \tag{A.32}$$

$$t(x, y) = e^{jkn\tau_0} e^{-j\frac{k}{2f}(x^2+y^2)}. \tag{A.33}$$

This expression represents the transmittance function of the lens. This equation describes the spatial phase transformation of the incident electromagnetic wave onto the lens. Note that the sign of the focal length may be positive for a converging lens, or negative for a diverging lens.

A.4.2 *Fourier transforming properties of lenses*

Now that it has been demonstrated how a lens modifies the phase of an incident electromagnetic wave, we will investigate how the phase transforming property affects the diffraction pattern observed at the focal plane of the lens placed in front of some arbitrary aperture illuminated by plane waves. The lens is placed a distance d in front of the aperture which is assumed to be in the Fresnel region of the aperture. The observation plane is at the focal plane of the lens as described in Figure A.8

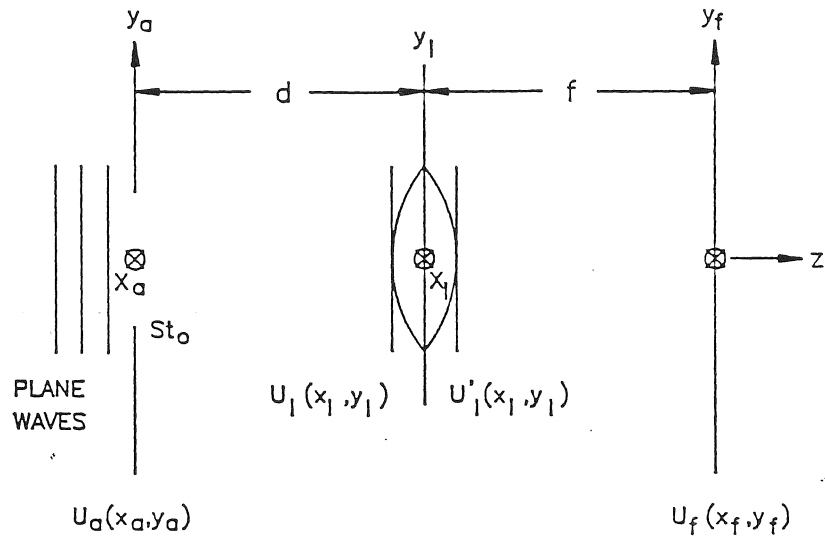


Figure A.8 Geometry for illustrating how a lens takes the Fourier transform of the incident aperture distribution.

With this arrangement, a point in the aperture plane is defined by the coordinates (x_a, y_a) , and a point in the observation plane at the focal plane of the lens by (x_f, y_f) . The aperture distributions of the electromagnetic field on the front plane and on the back plane of the lens are defined as $U_l(x, y)$ and $U'_l(x, y)$ respectively. (Note that the front and back planes are defined as the planes perpendicular to the axis including the point where the surface of the lens meets the optical axis). The transmittance function of the aperture is given by $U_a(x_a, y_a)$, which describes the amplitude of the disturbance function at the aperture plane. The aperture distribution incident towards the lens is given by the Rayleigh–Sommerfeld diffraction formula, and assuming that the lens is in the Fresnel region of the aperture so that the Fresnel approximation may be applied,

$$U_l(x, y) = \frac{e^{jkd}}{j\lambda d} \iint_{-\infty}^{\infty} U_a(x_a, y_a) e^{j\frac{k}{2d}[(x_a-x)^2+(y_a-y)^2]} dx_a dy_a \quad (\text{A.34})$$

$$= \frac{e^{jkd}}{j\lambda d} e^{j\frac{k}{2d}(x^2+y^2)} \times \iint_{-\infty}^{\infty} U_a(x_a, y_a) e^{j\frac{k}{2d}(x_a^2+y_a^2)} e^{-j\frac{k}{d}(xx_a+yy_a)} dx_a dy_a \quad (\text{A.35})$$

The aperture distribution on the back surface of the lens $U'_l(x, y)$ is found by multiplying $U_l(x, y)$ by the thickness function of the lens eq. (A.33):

$$U'_l(x, y) = e^{jkn\tau_0} e^{-j\frac{k}{2f}(x^2+y^2)} U_l(x, y) \quad (\text{A.36})$$

The $e^{jkn\tau_0}$ term in eq. (A.36) will be dropped, since it only adds a constant phase shift. Dropping this term will make the following expressions less complicated. –Just don't forget that it's there. Substituting in the expression for the aperture distribution $U_l(x, y)$ (eq. (A.44)), the $e^{j\frac{k}{2d}(x^2+y^2)}$ term cancels out. Thus,

$$U'_l(x, y) = \frac{e^{jkd}}{j\lambda d} \iint_{-\infty}^{\infty} U_a(x_a, y_a) e^{j\frac{k}{2d}(x_a^2+y_a^2)} e^{-j\frac{k}{d}(xx_a+yy_a)} dx_a dy_a \quad (\text{A.37})$$

The aperture distribution at the focal plane of Figure A.8 is given by applying the Fresnel diffraction formula again. This time, the aperture distribution is on the back surface of the lens $U'_l(x, y)$.

$$U_f(x_f, y_f) = \frac{e^{jkf}}{j\lambda f} \iint_{-\infty}^{\infty} U'_l(x, y) e^{j\frac{k}{2f}[(x_f-x)^2+(y_f-y)^2]} dx dy$$

$$\begin{aligned}
U_f(x_f, y_f) &= \frac{e^{jkf}}{j\lambda f} e^{j\frac{k}{2f}(x_f^2+y_f^2)} \times \\
&\int\int_{-\infty}^{\infty} U'_i(x, y) e^{j\frac{k}{2d}(x^2+y^2)} e^{-j\frac{k}{d}(xx_f+yy_f)} dx dy \quad (\text{A.38})
\end{aligned}$$

Substituting in for $U'_i(x, y)$, we end up with a formidable expression:

$$\begin{aligned}
U_f(x_f, y_f) &= -\frac{e^{jk(f+d)}}{\lambda^2 f d} e^{j\frac{k}{2f}(x_f^2+y_f^2)} \\
&\cdot \int\int_{-\infty}^{\infty} \left\{ \int\int_{-\infty}^{\infty} U_a(x_a, y_a) e^{j\frac{k}{2d}(x_a^2+y_a^2)} e^{-j\frac{k}{d}(xx_a+yy_a)} dx_a dy_a \right\} \\
&\cdot e^{j\frac{k}{2f}(x^2+y^2)} e^{-j\frac{k}{f}(xx_f+yy_f)} dx dy \quad (\text{A.39})
\end{aligned}$$

After regrouping terms,

$$\begin{aligned}
U_f(x_f, y_f) &= -\frac{e^{jk(f+d)}}{\lambda^2 f d} e^{j\frac{k}{2f}(x_f^2+y_f^2)} \\
&\cdot \int\int_{-\infty}^{\infty} \left\{ \int\int_{-\infty}^{\infty} U_a(x_a, y_a) e^{j\frac{k}{2d}(x_a^2+y_a^2)} dx_a dy_a \right\} \\
&\cdot e^{j\frac{k}{2f}[x^2-2x(x_f+\frac{f}{d}x_a)+y^2-2y(y_f+\frac{f}{d}y_a)]} dx dy \quad (\text{A.40})
\end{aligned}$$

Completing the square on the outer integral,

$$\begin{aligned}
U_f(x_f, y_f) &= -\frac{e^{jk(f+d)}}{\lambda^2 f d} \int\int_{-\infty}^{\infty} \left\{ \int\int_{-\infty}^{\infty} U_a(x_a, y_a) e^{-j\frac{k}{2f}(1-\frac{f}{d})(x_a^2+y_a^2)} \right. \\
&\cdot \left. e^{-j\frac{k}{d}(xx_a+yy_a)} dx_a dy_a \right\} e^{-j\frac{2}{2f}\cdot\frac{k}{2f}[(x-(x_f+\frac{f}{d}x_a))^2+(y-(y_f+\frac{f}{d}y_a))^2]} dx dy \quad (\text{A.41})
\end{aligned}$$

Multiplying the top and bottom of the exponent by 2 in eq. (A.41) allows us to express the outside integrals in the form of Fresnel integrals. Letting

$$u = \sqrt{\frac{2}{\lambda d}} \left[x - \left(x_f + \frac{f}{d} x_a \right) \right]; \quad v = \sqrt{\frac{2}{\lambda d}} \left[y - \left(y_f + \frac{f}{d} y_a \right) \right]$$

$$du = \sqrt{\frac{2}{\lambda d}} dx; \quad dv = \sqrt{\frac{2}{\lambda d}} dy$$

$$U_f(x_f, y_f) = -\frac{e^{jk(f+d)}}{2\lambda d} \iint_{-\infty}^{\infty} e^{-j\frac{\pi}{2}u^2} e^{-j\frac{\pi}{2}v^2} dudv$$

$$\cdot \iint_{-\infty}^{\infty} U_a(x_a, y_a) e^{-j\frac{k}{2f}(1-\frac{f}{d})(x_a^2+y_a^2)} e^{-j\frac{k}{d}(xx_a+yy_a)} dx_a dy_a \quad (\text{A.42})$$

Although the outer integrals are a set of indefinite Fresnel integrals, they may be solved in closed form. The solution to each of these integrals is found to be $(1+j)$, and since there are two integrals we end up with $(1+j)^2$ or $2j$. Therefore,

$$U_f(x_f, y_f) = \frac{jk(f+d)}{j\lambda d} \times$$

$$\iint_{-\infty}^{\infty} U_a(x_a, y_a) e^{-j\frac{k}{2f}(1-\frac{f}{d})(x_a^2+y_a^2)} e^{-j\frac{k}{d}(xx_a+yy_a)} dx_a dy_a \quad (\text{A.43})$$

Finally, if we let $d=f$, we end up with an exact Fourier transform relationship between $U_f(x_f, y_f)$ and $U_a(x_a, y_a)$.

$$U_f(x_f, y_f) = \frac{e^{j2kf}}{j\lambda f} \iint_{-\infty}^{\infty} U_a(x_a, y_a) e^{-j\frac{k}{f}(xx_a+yy_a)} dx_a dy_a \quad (\text{A.44})$$

BIBLIOGRAPHY

- [1] Ruze, John "Antenna Tolerance Theory—A Review," *Proc. IEEE*, vol. 54, pp. 633–640, Apr. 1966
- [2] von Hoerner, Sebastian, "The Design of Correcting Secondary Reflectors," *IEEE Transactions on Antennas and Propagation*, AP-24, pp. 336–340, May, 1976
- [3] von Hoerner, Sebastian and Wong, Woon-Yin, "Gravitational Deformation and Astigmatism of Tilttable Radio Telescopes," *IEEE Transactions on Antennas and Propagation*, AP-23, pp. 317–323, Sept. 1975
- [4] Mast, Terry, S. and Nelson, Jerry, E. "Figure Control for a Fully Segmented Telescope Mirror," *Applied Optics*, vol. 21, pp. 2631–2641, Jul. 1982
- [5] Sinnott, Roger, W. "The Keck Telescope's Giant Eye," *Sky and Telescope*, vol. 84, pp 15–22, Jul. 1990
- [6] Iizuka, Keigo. Engineering Optics. Berlin, New York: Springer-Verlag, 1983.
- [7] Tuovinen, J., Hirvonen, T.M., Räsänen, A. "Near-Field Analysis of a Thick Lens and Horn Combination: Theory and Measurements," *IEEE Transactions on Antennas and Propagation*, AP-40, pp. 613–619, Jun. 1992
- [8] Goodman, Joseph W., Introduction to Fourier Optics. New York: McGraw Hill, 1968.
- [9] Born, Max and Wolf, Emil. Principles of Optics, 6th ed. London, G.B., Pergamon Press, 1980.